2019

Documentation and analysis of plastic fingerprint impressions involving contactless three-dimensional surface scanning

BOSTON UNIVERSITY

SCHOOL OF MEDICINE

Thesis

DOCUMENTATION AND ANALYSIS OF PLASTIC FINGERPRINT

IMPRESSIONS INVOLVING CONTACTLESS THREE-DIMENSIONAL

SURFACE SCANNING

by

WUCHEN ZHANG

B.Sc., McGill University, 2017

Submitted in partial fulfillment of the

requirements for the degree of

Master of Science

2019

Approved by

First Reader   _____

                      Amy N. Brodeur, M.F.S.
                      Assistant Professor, Program in Biomedical Forensic Sciences
                      Department of Anatomy & Neurobiology

Second Reader   _____

                      Marzena Mulawka, M.F.S.
                      Instructor, John Jay College of Criminal Justice
                      City University of New York

Third Reader   _____

                      Deborah Kosiorek, M.S.
                      Criminalist IV, Latent Print Unit
                      Boston Police Department

ACKNOWLEDGMENTS

DOCUMENTATION AND ANALYSIS OF PLASTIC FINGERPRINT IMPRESSIONS INVOLVING CONTACTLESS THREE-DIMENSIONAL SURFACE SCANNING

WUCHEN ZHANG

ABSTRACT

Fingerprint impressions are frequently encountered during the investigation of crime scenes, and may establish a crucial linkage between the suspect and the crime scene. Plastic fingerprint impressions found at crime scenes are often transient and delicate, leaving photography the sole means of documentation. A traditional photography approach can be inadequate in documenting impressions that contain three-dimensional (3D) details due to the limitations of camera and lighting conditions on scene. In this study, 3D scanning was proposed as a novel method for the documentation of plastic fingerprints. Structured-light 3D scanning (SLS) captures the distortion of projected light patterns on the subject to obtain its 3D profile, which allows fast acquisition of the complete 3D geometric information of the surface. The contactless operation of SLS also eliminates the risk of destroying fragile evidence, making it a sound choice for forensic applications.

In this study, the feasibility of 3D scanning of plastic fingerprint impressions was evaluated and compared with traditional photography regarding the quantity and quality of perceptible friction ridge features. Attempts were made to develop a procedure to extract curvature features from 3D scanned fingerprints and flatten the friction ridge features into two-dimensional (2D) images to allow direct comparison with the traditional photography

method in the CSIpix® Matcher and NFIQ 2.0 software. One of the developed methods (3DR) utilizing a discrete geometry operator and convexity features outperformed traditional photography, both in minutiae count and match quality, while traditional photography could not always capture enough high-quality minutiae for comparisons, even after digital enhancement. The reproducibility of the 3D scanning process was evaluated using 3D point cloud statistics. The pair-wise mean distance and standard deviation were calculated for four levels of comparisons with theoretically increasing disparity, including pairs of scans of the same impressions. The results showed minimal shape deviation from scan to scan for the same impression, but high variations for different impressions.

TABLE OF CONTENTS

<div align="right">Page</div>

LIST OF TABLES

LIST OF FIGURES

LIST OF ABBREVIATIONS

2D   Two-Dimensional

2EP   Enhanced 2D Photographs

2UP   Unenhanced 2D Photographs

3CB   Blue channel image of extracted 3D features using Classic operator

3CR   Red channel image of extracted 3D features using Classic operator

3D   Three-Dimensional

3DB   Blue channel image of extracted 3D features using Discrete operator

3DR   Red channel image of extracted 3D features using Discrete operator

AFIS   Automated Fingerprint Identification System

B.C.   Before Christ

DPI   Dot-per-inch

DSLR   Digital Single-Lens Reflex

EGA   Estimated Gestational Age

NFIQ2   NIST Fingerprint Image Quality 2.0

NIST   National Institute of Standards and Technology

NL   Newfoundland and Labrador

RGB   Red, Green, Blue

SLS   Structure-Light Scanning

STL   Stereolithography

TIF   Tag Image Files

UI   User interface

1. INTRODUCTION

1.1 Fingerprint Overview

1.1.1 History of Fingerprint Identification

The practice of using fingerprints for personal identification has become commonplace in the past century, ranging from solving crimes to securing a smart electronic device. The earliest observation of such practice has been said to originate from China as early as 221 B.C., where deeds and other legal documents were found to bear marks made by a fingertip and sometimes the entire palm[1–3]. Sir William Herschel, a British administrator in India, observed the practice of putting a fingerprint beside a signature on contracts from local people, and in 1860 he began to promote the use of fingerprinting to prevent false impersonation and contract disputes[4]. While claiming to be the first person to use fingerprints for personal identification purposes, Herschel also tirelessly collected his own handprints and others over a 57-year interval to demonstrate the "stubborn persistence of the patterns on our fingers"[5]. Herschel's collection was then passed on to Sir Francis Galton, who consolidated the pioneering works into a more comprehensive study, which was the first to demonstrate the effect of injuries on fingerprints as well as the restoration of the skin pattern after a superficial burn[6].

Although the claims to priority are open to debate[5,7], it is commonly agreed that it was not until *People v. Jennings*[8] that fingerprint identification gained its place in the criminal justice arena in the United States. On December 21, 1911, the Illinois Supreme Court cited the historical record and determined the use of fingerprints as a reliable means of identification. However, the first American courts to decide the admissibility of

1

fingerprint evidence failed to scrutinize the scientific legitimacy of the method and essentially admitted forensic fingerprint evidence because it was accepted in British courts[9]. Fingerprint evidence kept accumulating judicial legitimacy from its longstanding use in the courts until the advent of the *Daubert* standard in 1993[10] and the publication of the National Academy of Sciences (NAS) report in 2009[11]. Despite increasing admissibility challenges, fingerprint evidence still provides invaluable service to the criminal justice system and fingerprints recovered during criminal investigations are often crucial pieces of evidence that establish linkage between suspects and crime scenes.

1.1.2 Biology of Friction Ridge Skin

Human volar skin, or skin pertaining to the sole or the palm, consists of two main layers: the outer layer, or epidermis, and the inner layer, or dermis [Figure 1]. The epidermis and dermis are separated by a basement membrane, or the basal lamina, which acts as the linkage and the barrier between the two tissue layers. The basal layer of epidermal cells is often referred to as the *generating layer* given its key role in constantly generating new epidermal cells, which slowly push toward the surface and replace older cells[4]. The dermis is a matrix of loose connective tissue composed of fibrous proteins. The dermis serves the function of supplying nutrients to the epidermis as well as providing physical protection to the internal tissues. Through mammalian evolution, ridges of rows of modified scales are fused into a specialized layer of friction skin, later named friction ridges, which form at right angles to the friction force to reduce slippage[12]. In the case of pointed pads, such as fingertips, friction ridges are arranged in concentric circles around

the summit of the volar pads. The path of surface friction ridges corresponds to rows of blunt peg-like structures on the dermis called dermal papillae, where the ridges or folds of the basal layer corresponding to the surface ridges of friction skin are termed primary ridges. Ridges alternating between primary ridges are termed secondary ridges and correspond to the furrows on the surface of friction skin[13].

In humans, primary ridges start to form at approximately 10.5 weeks estimated gestational age (EGA), and sweat glands, which later create exits through the sweat pores on the epidermis, begin to appear at 14 weeks EGA. As the finger grows in utero, the ridges actively multiply to keep pace with the growth, forming new primary ridges across the finger and separating the existing primary ridges[14]. Bifurcations form when new ridges pull away from existing primary ridges. Ridge endings form when a developing ridge becomes sandwiched between two established ridges. While primary ridges mature and extend deeper into the dermis, secondary ridges begin to form between 15 and 17 weeks EGA, forming the furrows on the surface of friction ridge skin. The minutiae within the fingerprint pattern become permanently set once secondary ridge formation begins, and only increase in size during maturity at about 24 weeks EGA[13]. The persistence and uniqueness of friction ridge patterns rely on the unique cellular attachment of the skin components as well as the consistent rate at which basal cells produce new epidermal cells. Injury or disease that does not penetrate deeply enough to damage the dermis will be eventually repaired by the proliferating basal cells. Genetic information ultimately provides the blueprint for the arrangement of friction ridge patterns. However, like any other biological process, the development of friction ridges depends on many extrinsic and

intrinsic factors. Even in monozygotic twins who share identical genetic makeup, the minutiae on their fingerprints still bear variations[15].
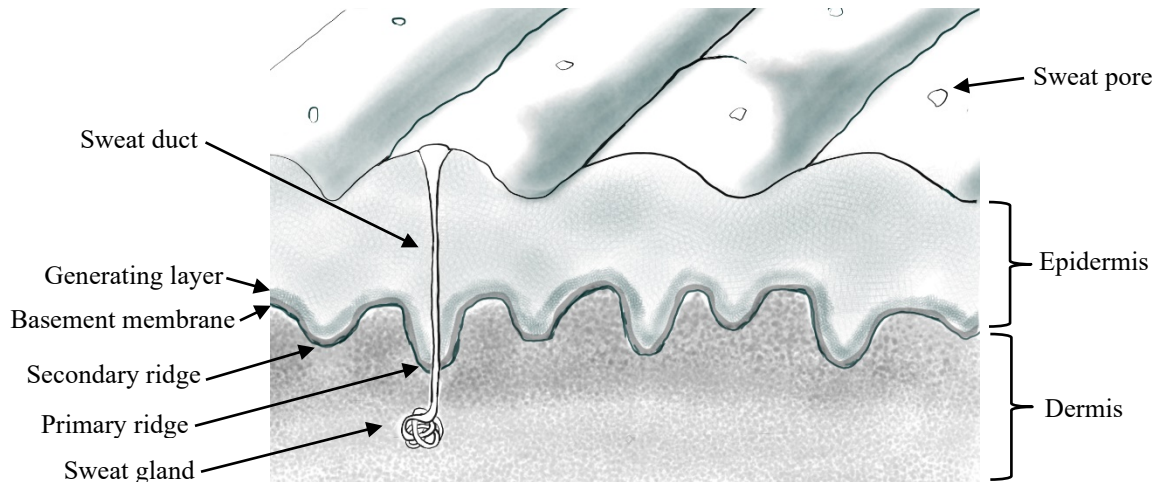
Figure 1. Illustration of the structure of friction ridge skin.

1.2 Fingerprint Evidence

1.2.1 Development, Collection, and Enhancement

Friction ridge analysis entails the detection, collection, and examination of impressions created from friction ridge skin, and falls under the discipline of pattern evidence. Fingerprint evidence is based upon three major premises: (1) The uniqueness of individual friction ridge patterns; (2) the permanence of friction ridges throughout a person's life; and (3) the tendency of individuals to transfer an impression of friction ridges to another surface. Fingerprint impressions of probative value are frequently encountered during the investigation of crime scenes. Recovered fingerprints are classified into three major types: latent, patent, and plastic[16]. Patent prints are the visible fingerprints impressed onto a surface and usually do not require enhancement, as the chemical composition of

these prints can be any material that creates a contrast with the background. Latent prints are fingerprints that are not readily visible to the naked eye, and often require additional physical or chemical processes to visualize, enhance, and preserve them (e.g., black fingerprint powder on a white tile, superglue fuming on an irregular surface). Powdered prints can be collected using a tape lift or a gel lift depending on the shape of the surface. Since latent prints are mainly composed of eccrine sweat, which is made of approximately 99% water and 1% solid components[4], targeted reagents such as ninhydrin and iodine can be used to react with a specific component of the latent print residue, forming a colored compound to reveal friction ridge details[3]. Photographic documentation with a digital single-lens reflex (DSLR) camera is required before and after the development of patent and latent prints to ensure the integrity of the evidence. Plastic prints are friction ridge impressions left in a soft, malleable surface, such as putty and chewing gum[3]. In contrast to the two-dimensional (2D) latent and patent prints, a plastic print is a three-dimensional (3D) preservation of friction ridge details. The conventional approach to documenting plastic prints at the crime scene is to photograph the impression under oblique light, which fills the ridges with shadows to create contrast. When the substrate is stable, it is also possible to create a cast of the impression, which could then potentially be inked and rolled onto a fingerprint card[17].

1.2.2 Challenges with Plastic Prints

While a vast amount of attention is devoted to the study of latent fingerprints, which has become the common name for the entire subdiscipline[3], there is a minimal number of

studies regarding the topic of plastic fingerprints. The best approximations are the published studies on 3D fingerprint identification[18–21], but these studies generally concentrate on developing new finger-scanning methodologies to implement in biometric fingerprint scanners and do not deal with the complexity of crime scenes or the different physical properties of plastic fingerprint substrates. Meanwhile, plastic fingerprint impressions (e.g. "impressions left upon a thick clot of varnish"[6]) can be transient and delicate, posing challenges for collection, transportation, and storage. In these cases, the analysis of fingerprints relies solely on the photographic documentation obtained during crime scene processing. The traditional photography approach tends to be affected by a large range of factors such as lighting condition, camera angle, and distance. A scale or ruler is typically required to be alongside the impressions and placed at the same level as the impression so that the camera can focus on both the impression and the scale. The requirement is intuitive for a 2D impression on a flat surface, but for a 3D impression on a curved surface, it is often not applicable. It is also difficult to reliably measure the depth of the friction ridges without direct contact with the impression. The depth details of a 3D impression often demand an f-stop setting high enough to obtain a high depth of field, yet as low as possible to minimize lens aberrations. Such fine adjustments can require a significant amount of time and effort, which is only further complicated by unpredictable lighting conditions.

1.2.3 Friction Ridge Impression Examination (ACE-V)

In the United States, fingerprint features are generally categorized into three levels [Figure 2]. Level 1 features are known as the loop, the whorl, and the arch, which are the three ridge flow patterns established by Francis Galton[3]. He was also the first to describe Level 2 features known as minutiae, which include features such as ridge endings and bifurcations[22]. Level 3 features include all the dimensional attributes of friction ridges such as width, ridge shape, and pores. When combined with Level 1 and Level 2 features, Level 3 features provide significant discriminatory value[23]. Latent print examiners carry out comparison tasks following the ACE-V methodology[24,25], which entails the process of analysis, comparison, evaluation, and verification. During the analysis phase, the examiner determines the suitability of a fingerprint for comparison purposes based on the quantity and quality of details observed. If determined to be suitable, side-by-side comparison of all levels of detail is performed to assess disagreement or agreement between the impressions. Based on the disagreement or agreement observed, the examiner forms one of the three conclusions (exclusion, identification, and inconclusive) in the evaluation phase or returns to the analysis phase to reassess suitability. Even though the count of the corresponding minutia is often utilized as the predominant discriminative factor by examiners in the United States[26], no minimum number of features is required for an identification decision. Due to the subjective nature of fingerprint examination, the ACE process is applied by a subsequent examiner in the verification phase to either support or reject the conclusions of the original examiner.

LEVEL 1 FEATURES

| ARCH | TENTED ARCH | LEFT LOOP | RIGHT LOOP | DOUBLE LOOP | WHORL |

LEVEL 2 FEATURES

| LINE-UNIT | LINE-FRAGMENT | ENDING | BIFURCATION | EYE | HOOK |

LEVEL 3 FEATURES

| PORES | LINE SHAPE | INCIPIENT RIDGES | CREASES | WARTS | SCARS |
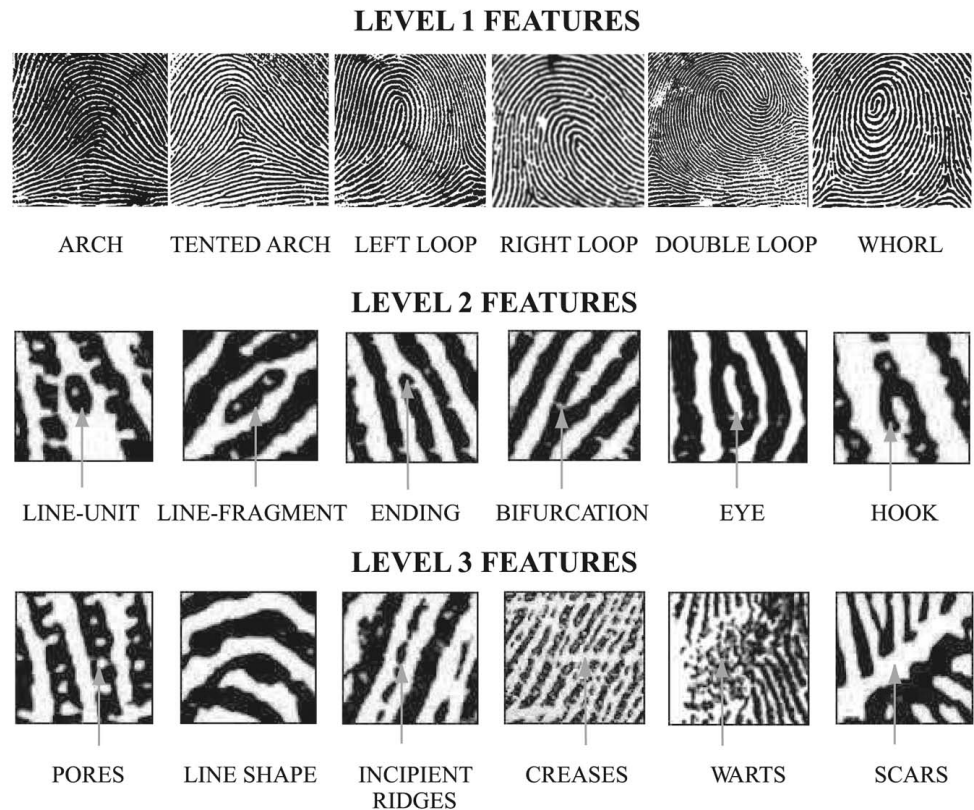
Figure 2. Examples of Level 1, Level 2, and Level 3 fingerprint features[23].

1.3 Structured-Light 3D Scanning

1.3.1 Principle of 3D Reconstruction

Originating from the study of computer vision[27], 3D reconstruction technology is attracting growing interest from the forensic community. The goal of 3D reconstruction, or 3D digitalization, is to extract the three-dimensional geometric information and possibly other physical features (e.g., texture, color, and reflectance) from captured images of a real-world scene and reconstruct them into a 3D model in the digital realm. Depending on the specific application, these 3D data could be acquired by a plethora of methods and technologies including photogrammetry[28], laser sensors[29], and magnetic resonance imaging[30]. With the power of computer programs, the acquired pieces or slices of 3D

8

information can be recognized, re-organized, and joined into one continuous 3D object. Triangular meshes are a common way to represent a 3D object, which are acquired by connecting the points in 3D space to their neighbouring points to form a collection of vertices, edges, and faces [Figure 3]. The collection of vertices is also referred to as a point cloud, which contains solely the raw data points from the 3D scan. Limitations vary with technique and hardware, but optical 3D scanners are known to struggle with shiny, reflective, and transparent surfaces[31].
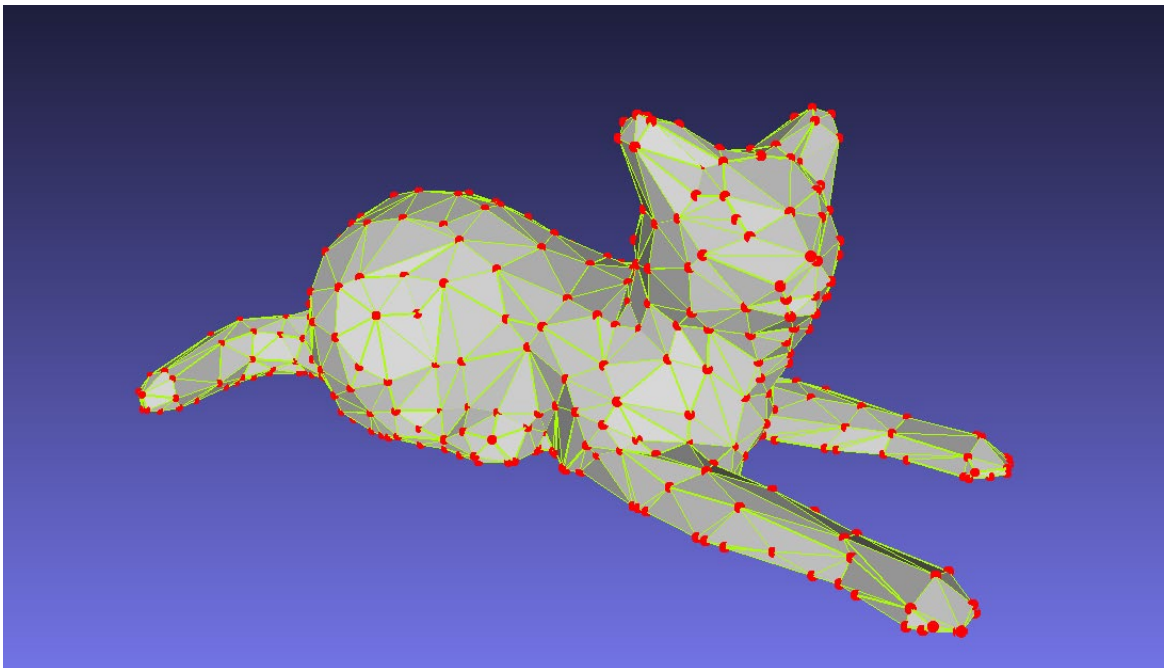
Figure 3. Triangular mesh representation of a 3D model of a cat. In a triangular mesh model, the vertices are connected by the edges, which enclose the faces. Image adapted from *Low Poly Cat* by slavikk, licensed under the Creative Commons - Attribution - Non-Commercial - Share Alike license (https://www.thingiverse.com/thing:908621).

1.3.2 Mechanism of Structured-Light Scanning

Structured-light 3D scanning (SLS) utilizes the distortion of projected light patterns on the subject to obtain its 3D surface profile[32]. As a powerful tool for rapid recording and measuring of 3D surface features, SLS-based techniques have already been researched and adopted by the forensic community for documenting open wounds[33], osteological trauma[34], obtaining 3D fingerprints from live individuals[35], and recording postmortem fingerprints[36]. The hardware of a low-budget structured-light scanner can be as minimal as a video projector, a digital camera, and a computer that runs algorithms to process the captured images[37]. The video projector serves as the light source that projects patterns of light on the subject. Depending on the technique, the light pattern can take the form of stripes, grids, phase shifts, rainbows, or some of these combined in a sequential projection[32,38]. The deformation of light patterns by the subject is recorded by the digital camera, which is then processed by a computer program to calculate the distance of each point by triangulation between the distorted and original patterns [Figure 4]. Unlike laser scanners that only scan one point per time, SLS scans the full field of view at once, which significantly boosts the scanning speed and eliminates noise from motion[31]. Due to the dependence on the projection of light patterns, SLS is commonly utilized for 3D scanning of objects or scenes of small to medium size.
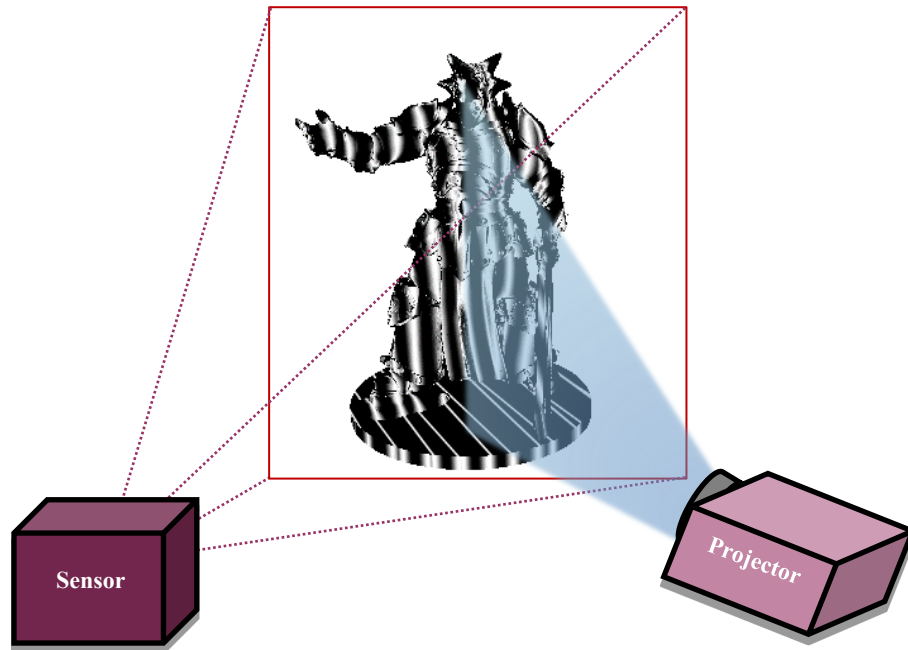
Figure 4. Illustration of a structured-light scanning (SLS) system. A pattern of light (black and white stripes) is emitted from the projector and distorted by the object, then captured by the light sensor or camera. Image adapted from *D&D Dragonborn Paladin* by doesntfearzeus, licensed under the Creative Commons - Attribution - Non-Commercial - Share Alike license (https://www.thingiverse.com/thing:3134625).

1.4 Study Purpose

The purpose of this study was to investigate the feasibility of structured-light 3D scanning for the documentation of plastic prints and compare its quality to traditional crime scene photography. In order to conduct the evaluation using the same criteria, the study also attempted to develop a method based solely on open-source software to extract friction ridge information from digitalized 3D fingerprint impressions. The method allowed side-by-side comparison of 3D scanned impressed prints with rolled prints as well as the usage of automated fingerprint feature detection software for minutiae-based fingerprint analysis. The quality of collected fingerprint impressions was estimated by three different scores: minutiae count, match score, and NFIQ2 score. NFIQ2 score is a software-assigned quality

11

score for a fingerprint image which aggregates a range of individual quality scores including image clarity, fingerprint size, minutiae count and minutiae quality. Fingerprint images of higher quality were expected to contain more minutiae, therefore a higher match score and a higher NFIQ2 score. Depending on the 3D scan resolution and accuracy, the 3D features of friction ridges could also aid the identification process. If proven successful, 3D scanning could potentially reinforce or replace traditional photography in the documentation of 3D-detailed impression evidence.

2. MATERIALS AND METHODS

2.1 Preparation of Plastic Prints

A volunteer's right thumb was chosen to be the main template finger for this series of experiments owing to its relatively large size and a rather uncommon double-loop whorl pattern [Figure 5]. The volunteer's left thumb was used as a negative control during the 3D shape comparisons. All impressions were contained in 5 mL aluminum cans with a lid and then placed in a Pelican™ 1200 case (Pelican Products, Torrance, California) for storage [Figure 6]. Twenty different materials were collected based on availability [Table 1]. The twenty materials can be grossly divided into three groups based on the ease of fingerprint deposition. Group A (chewed gum, dental silicone putty, plumber's putty, pomade, modeling putty) did not require additional processes before deposition of fingerprints. The template finger was firmly pressed into each material and lifted gently to deposit as much detail as possible. For oily or viscous materials, the finger was moistened before pressing. Group B (dental stone, acrylic paints, nail polish, soap, Mikrosil™) required additional effort with timing. Group B materials, once mixed or exposed to air, took several to tens of minutes to dry or settle to a state at which fingerprint deposition was possible and would then solidify. Since the timing also depended on various extrinsic factors such as thickness, surface area, and environmental temperature, fingerprint depositions on Group B materials were attempted in a best effort manner. Group C (sealing wax, candle waxes, dental modeling compounds) all required heat to melt the material prior to deposition of fingerprints. The materials were melted at near 100 degrees Celsius within their individual aluminum containers and allowed to cool at room temperature. After 5-10 minutes, the

template finger was impressed into a pool of melted material until it solidified. If the impression quality was acceptable and the quantity of the material was sufficient, additional impressions in the material were produced. Among Group A, B, and C, 21 impressions in 11 different materials were selected for downstream experiments.

Table 1. List of materials tested for retention of plastic prints. Opacity and reflectance are simplified into binary values (Yes and No). If any level of translucency was observed for a material, its opacity was classified as *No*. If any bright reflective area was observed for a material, its reflectance was classified as *Yes*. Bolded materials were selected for subsequent experiments.

MATERIAL NUMBER	MATERIAL NAME	COLOR	OPACITY	REFLECTANCE
1	**Chewed gum**	Blue	Yes	Yes
2	**Dental modeling compound**	Red	Yes	No
3	**Plumber's putty**	Yellow	Yes	Yes
4	**Candle wax**	Black	Yes	Yes
5	**Candle wax**	Green	Yes	Yes
6	**Sealing wax**	Red	Yes	No
7	**Pomade**	Green	Yes	Yes
8	**Dental silicone putty**	Blue	No	No
9	**Modeling putty**	Gray	Yes	No
10	Dental stone	Pink	Yes	No
11	Acrylic paint	Red	Yes	No
12	Acrylic paint	White	Yes	No
13	Acrylic paint	Black	Yes	No
14	Crafting glue	White	No	Yes
15	Butter	Yellow	Yes	Yes
16	Nail polish	Pink	Yes	Yes
17	Nail polish	Clear	No	Yes
18	Wet soap	White	Yes	Yes
19	**Mikrosil™**	White	Yes	No
20	**Mikrosil™**	Brown	Yes	No

Figure 5. Inked fingerprints of a volunteer's left thumb (left) and right thumb (right). The two images are inked fingerprints scanned from a tenprint card. Both images have been calibrated, reoriented, digitally enhanced and used as reference impressions.

Figure 6. A container system for the storage and transportation of delicate plastic prints. A piece of dental silicone putty (left) containing a thumb impression was stored in a 5 mL aluminum container, which was placed in a PelicanTM 1200 case (right) for storage and transport. Cardboard backing was used for materials of limited quantity.

2.2 Lighting Setup and Photography

A general guideline of crime scene photography was followed for the photography of the fingerprint impressions. A Canon Rebel EOS T5i DSLR Camera with a 50mm lens (Canon Inc., Lake Success, New York) was installed on an MK Photo-eBox™ Digital Imaging System (MK Digital Direct, Chula Vista, California) [Figure 7]. The photo box was set to produce diffused white light, and the camera was set to aperture priority (Av) mode. Each 3D impression was left *in situ* within the aluminum container and placed in the photo box within the camera's center field of view. An L-shaped ruler was placed adjacent to the container and propped to the same horizontal plane as the impression [Figure 8]. Three photographs, referred to as a photoset, of each impression at three different orientations, were captured with manual focus. In total, 63 photographs of 21 impressions were captured [Table 2].
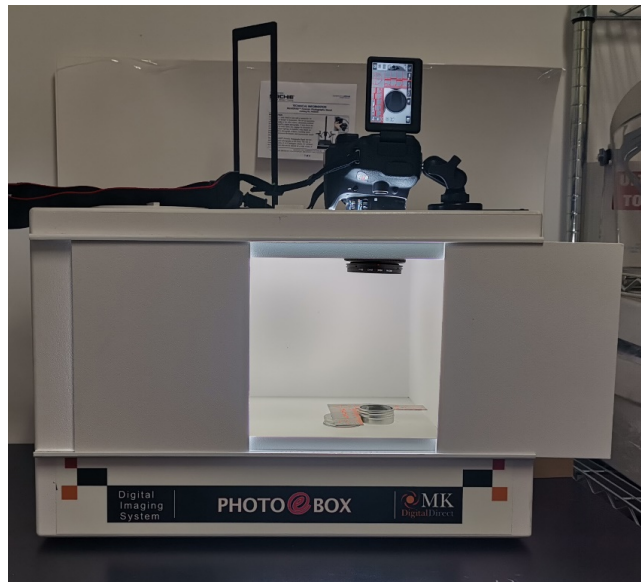
Figure 7. Setup of Canon DSLR camera with MK Photo-eBox ™ Digital Imaging System. The door in this photograph is kept open for visualization of internal setup, however the actual photographs were taken with both doors closed for optimal lighting condition.

Table 2. List of impressions created from various materials. Each photoset is comprised of three photographs of the impression in three different orientations under in diffused lighting. Scans 1-31 were captured with the inEos X5®. Scans 32 and 33 were captured with the Artec Space Spider.

Impression number	Material name	Thumb (Left/Right)	Photoset number	3D scan number
1	Black - candle wax	R	1	1
2	Chewed gum	R	2	2
3	Chewed gum	R	3	3
4	Dental silicone putty	R	N/A	4
5	Dental silicone putty	R	4	5
6	Modeling clay	L	5	6
7	Modeling clay	R	6	7
8	Modeling clay	R	7	8, 9
9	Modeling clay	R	8	10, 11
10	Green - candle wax	R	9	12
11	Green - candle wax	R	10	13
12	Pomade	R	11	14
13	Pomade	R	12	15
14	Plumber's putty	R	13	16
15	Red - dental modeling compound	L	14	17
16	Red - dental modeling compound	R	15	18
17	Brown - Mikrosil™	R	N/A	19, 20
18	Red - sealing wax	R	16	21
19	Red - sealing wax	R	17	22
20	Red - sealing wax	R	N/A	23
21	White - Mikrosil™	R	N/A	24, 25
22	White - Mikrosil™	R	18	26, 27, 32, 33
23	Brown - Mikrosil™	R	19	28, 29
24	White - Mikrosil™	R	20	30
25	White - Mikrosil™	L	21	31
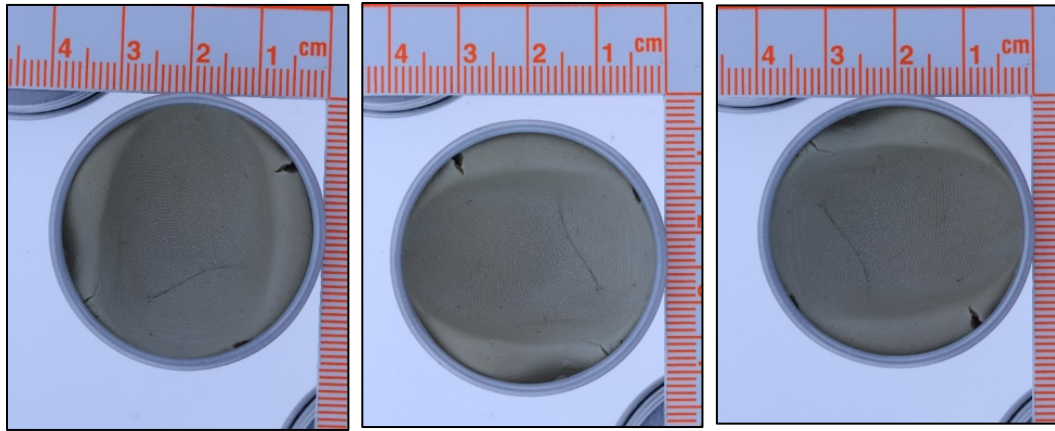
Figure 8. Triplicate photographs of a right thumb impression in plumber's putty under diffused white light. The impression was photographed along with its container, and an L-shaped ruler was supported to the same horizontal plane with the base plane of the impression.

2.3 3D Fingerprint Digitalization and Processing

2.3.1 3D Scanning with inEos X5®

The twenty-one impressions were transported to the Boston University Restorative Sciences and Biomaterials Laboratory (700 Albany St, Boston, MA) and scanned with a Dentsply Sirona inEos X5® (Sirona Dental Systems Gmbh, Bensheim, Germany). The inEos X5® unit is a commercially available benchtop 3D scanner utilizing blue structured-light scanning, and the system is designated for 3D digitalization of dental models and impressions. The scanner unit is accompanied with its software component Sirona Dental CAD/CAM System inLab SW Version 16.x (Sirona Dental Systems Gmbh, Bensheim, Germany), which processes the data captured by the sensor and reconstructs a 3D mesh model. As the system was designed exclusively for digital dentistry applications, the procedures for scanning fingerprint impressions were improvised according to the experience of the laboratory technician [Figure 9]. Each impression along with its container was fixed to a scanning platform using adhesive putty and placed within the scan area

[Figure 10]. The scan progress and the camera view could be visualized in real-time from the software user interface (UI) on the computer monitor [Figure 11].

A thin layer of CEREC Optispray (Sirona Dental Systems GmbH, Bensheim, Germany) was applied to lustrous materials as a standard protocol according to the manufacturer's instruction. Repeated scans were performed for two impressions in modeling putty, two impressions in brown Mikrosil™, and two impressions in white Mikrosil™ in order to study the reproducibility of 3D scanning methods. In total, 31 stereolithography (STL) files were obtained from the inEos X5®.

Step 1:   **Initiation**

At the "ADMINISTRATION" page, select "Model" then the "upper jaw" option to initiate a scan of a relatively large area.

Step 2:   **Scanning**

At the "SCAN" page, select the icon indicating "Capture Free" then "Capture Auto". Rotate or tilt the scanning platform to allow automatic scanning of multiple angles.

Step 3:   **Reconstruction**

Under "Model Options", select "Complete Reconstruction" for a 3D model with the best quality, then select the right arrow to proceed to the "MODEL" step.

Step 4:   **Export file**

At the "MODEL" page, select "Export" and save the model as "Standard STL file."
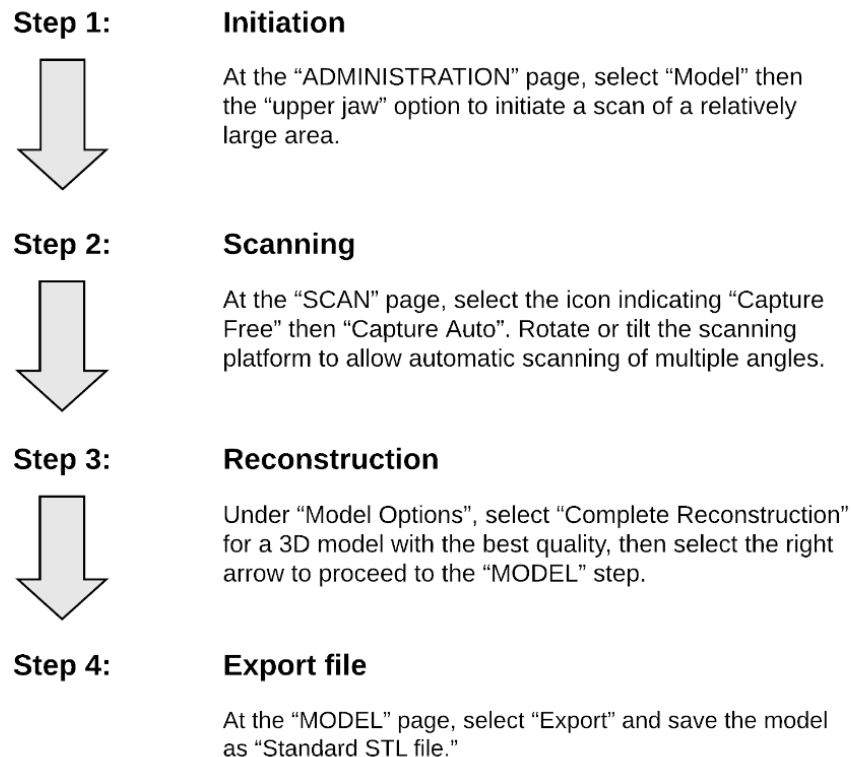
Figure 9. Steps for 3D scanning 3D fingerprint impressions with the inEos X5® unit. Generally, 10 to 15 scans of various angles were sufficient for capturing a fingerprint impression.
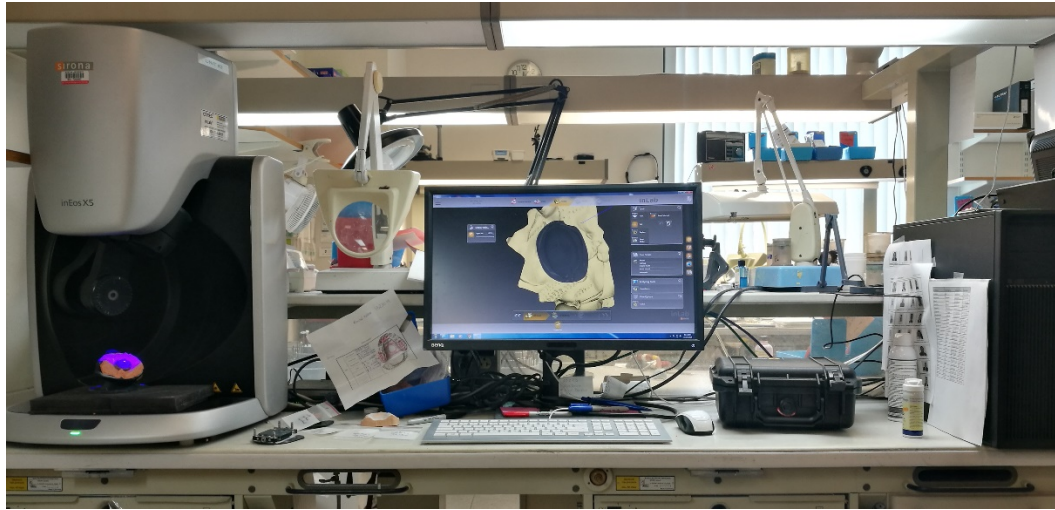
Figure 10. Setup of scanning platform using the free scan mode with the inEos X5® scanner unit. One right thumb impression in brown Mikrosil™ was attached to the top of the scanning platform and placed in the scan area (left). The scanner was connected to a computer (right), and the generated model could be viewed in real time on the monitor (middle). "Capture Free" mode was used in contrast with the automatic mode which utilizes the articulated arm to produce a finite number of orientations or scan angles.

Figure 11. The user interface (UI) of inLab SW 16.x during the scanning process. (a) Camera view from inEos X5®, (b) preview of the 3D model, (c) a series of previous partial scans to be merged, and (d) a gap between data indicating uncaptured area. The apparent irregularities on the fingerprint surface was due to the deformation of the material after deposition.

2.3.2 3D Scanning with Artec Space Spider

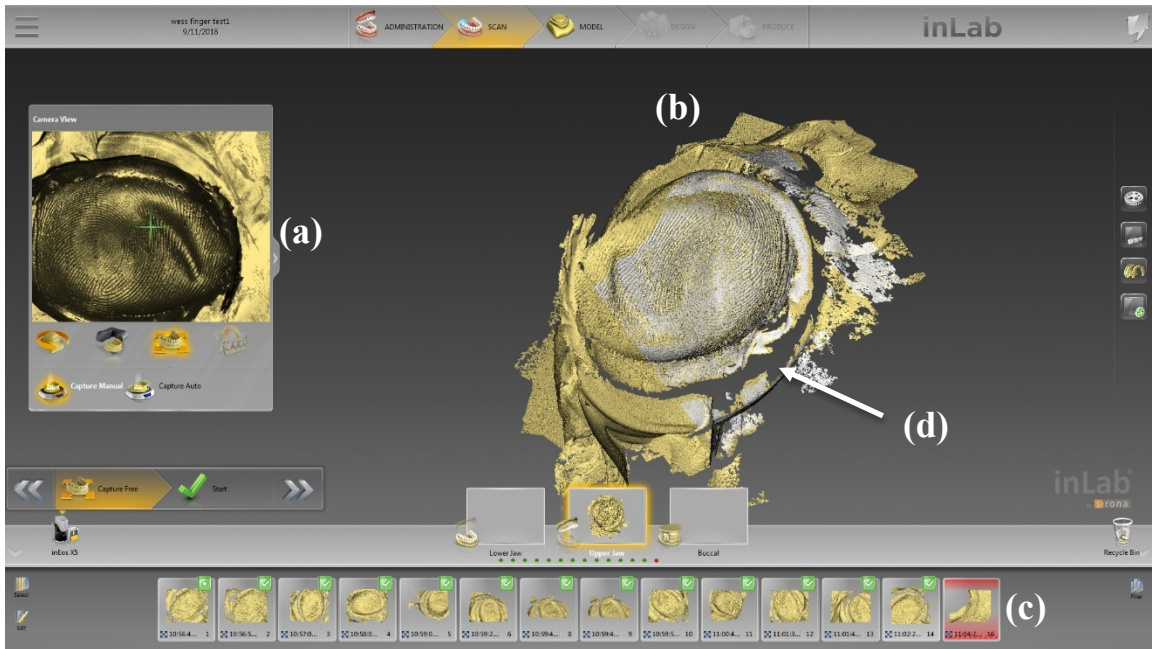One impression of the right thumb in white Mikrosil™ was shipped to Laser Design, Inc., Minneapolis, MN to be scanned with an Artec Space Spider 3D scanner (Artec Group, Luxembourg). The Artec Space Spider [Figure 12] is a handheld structured-light scanner that specializes in digitalizing small geometric details[39], and it also features simultaneous capture of colors and a high capture speed of up to 8 frames per second. Live demonstration of two scans of the impression, and the resulting STL and OBJ files were received.

Figure 12. Scanning of a 3D fingerprint impression using a handheld structured-light 3D scanner. The impression was taken out of its container and placed on a stand with reference markers. A turntable was used to adjust scan angles while the scanner was held still. The photograph was supplied courtesy of Laser Design, Inc.

2.3.3 Mesh Trimming

The 3D scanning process has limited ability to distinguish the scanned subject from its surroundings. Hence, extraneous information is usually captured during the scan. In this experiment, the aluminum container and the scanning platform were often included in the generated 3D model, which interfered with the calculations of surface geometries. CloudCompare Version 2.10 (GNU General Public License, retrieved from http://www.cloudcompare.org/), an open-source 3D point cloud processing software, was used to remove the redundant vertices in 3D scans. The 31 STL files from inEos X5® were imported into CloudCompare for two levels of mesh trimming. The first level of trimming was to remove the surrounding area and keep only the fingerprints [Figure 13]. The second level was to further remove scanning artifacts and material artifacts within the fingerprints to prepare mesh models for the 3D shape comparisons [Figure 14].
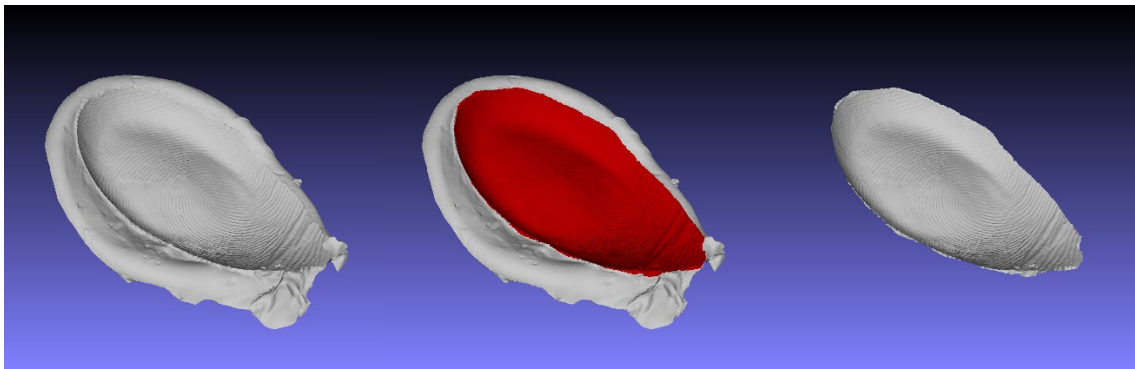

Figure 13. Illustration of the mesh trimming procedure. The fingerprint region (marked in red, middle) is selected on the original mesh model (left) and cropped out as an individual mesh model (right).
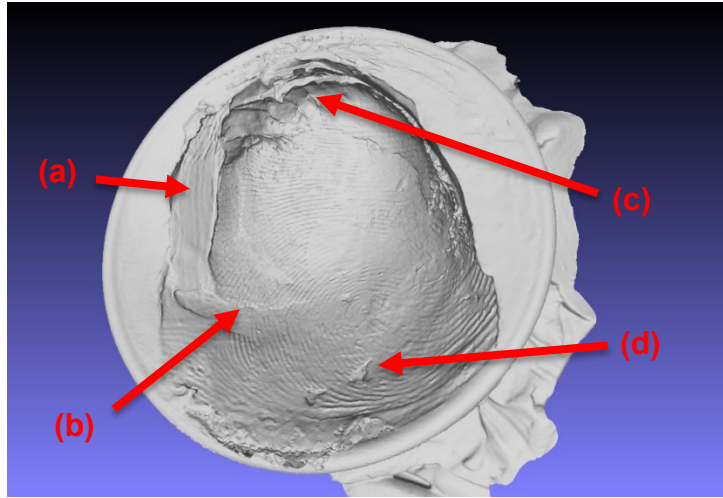
Figure 14. Example of artifacts embedded in the material (pomade). The depicted artifacts are: (a) a wipe, (b) a crease from layering of material, (c) ridges from pull-up of material, (d) holes in the material.

2.3.4 Curvature Features Extraction

Curvature describes how much a surface deviates from being a flat plane. Ridges and furrows in 3D fingerprint impressions are a perfect example of surface curvatures. The analytical methods for curvatures are deeply rooted in the mathematical discipline of differential geometry. The magnitude of curvature or the curvedness is defined as the absolute value of the reciprocal radius of the circle that best approximates the cross-section of that surface[40]. For each point on a surface, there exists a single normal curvature (i.e., curvature on an orthogonal plane to the surface point) with maximum curvedness, defined as k_1. The curvature perpendicular to k_1 is defined as k_2, while k_1 and k_2 are collectively called principle curvatures. The mean curvature k_H can be defined as the average of principle curvatures:

$$k_H = \frac{k_1 + k_2}{2}$$

23

The directionality of a curvature is derived from the mathematical equation of the circle that approximates the curvature cross-section, but for the simplicity of explanations, curvatures with an opening towards the outside of the surface (∪-shaped) are negative in direction, and curvatures with an opening towards the inside of the surface (∩-shaped) are positive in direction. The shape of a small surface can therefore be classified into five principal types based on the directions of k_1 and k_2 [Figure 15].
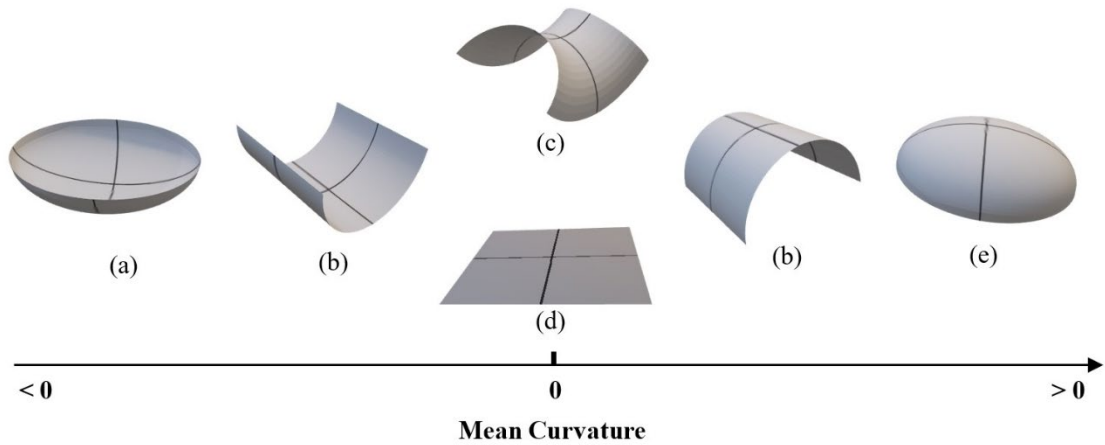
Figure 15. Basic classifications of surface features based on the directions of principal curvatures. Surface curvatures can be classified into (a) concavities ($k_2 < k_1 < 0$,), (b) parabolas ($k_1 = 0$ or $k_2 = 0$), (c) saddles ($k_2 < 0 < k_1$), (d) flat planes ($k_2 = k_1 = 0$), and (e) convexities ($0 < k_2 < k_1$).

Two differential geometry operators built in MeshLab[41] Version 2016 (Visual Computing Lab, ISTI-CNR, Pisa, Italy) were tested for the calculation of curvature features. One calculates curvature principle direction by pseudoinverse quadric fitting (Classic), and the second one calculates the mean curvature based on discrete differential geometry (Discrete) utilizing averaging Voronoi cells and demonstrates better accuracy with triangular meshes[42]. Both operators color-map each vertex or point based on its local mean curvature, where convexities are colored blue, concavities red, and flat or saddle-shaped

24

regions are green. In the context of plastic fingerprints, this scheme paints the friction ridges in red, furrows in blue, and flat regions in green [Figure 16]. However, the stacking of red, green, and blue (RGB) elements in one image can make visualization problematic, and Fiji[43] (ImageJ development team, Laboratory for Optical and Computational Instrumentation, University of Wisconsin-Madison), an open-source image processing and analysis software, was utilized for the separation of RGB color channels. The intensity of each color channel was converted to the intensity in grayscale. The combined process transformed 3D scanned fingerprints into their 2D equivalent of inked fingerprints, allowing downstream comparisons [Figure 17]. Only the first attempts of 3D scanning of each impression were processed for comparison to corresponding 2D photographs. The resulting fingerprint images are referred to as flattened 3D fingerprints.
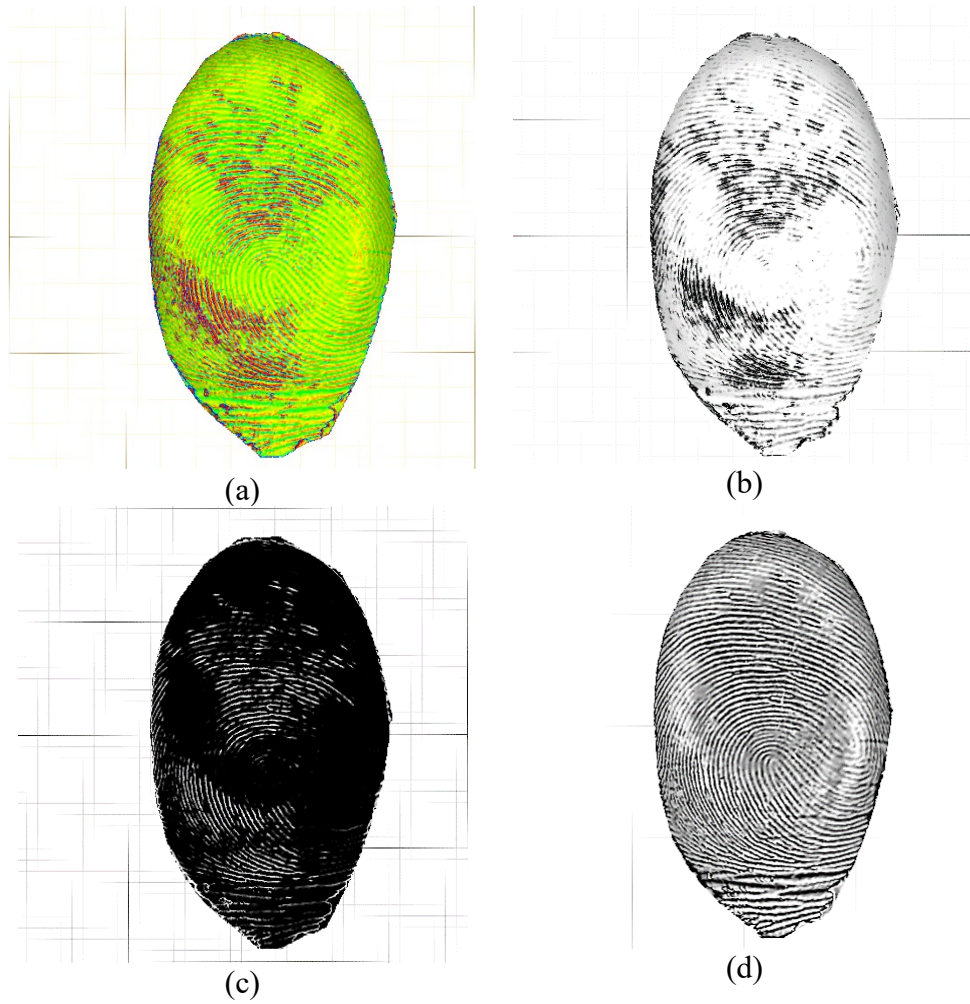
Figure 16. Color-mapped 3D mesh model and split RGB channels. This figure depicts (a) the result of curvature color-mapping with the classic operator, and (b) green, (c) blue, and (d) red channel images after RGB channel separation.
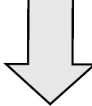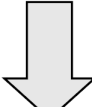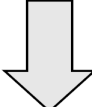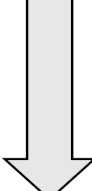
Step 1:   **Toggle orthographic view**

Open the STL file in MeshLab. Under the "View" menu, select "Toggle Orthographic Camera" to view the 3D model without depth perception.

Step 2:   **Toggle background grid**

Under "Render", select "Background Grid" to toggle the display of a 3D grid for downstream image calibration. The unit in the background grid is part of the scanner parameters.

Step 3:   **Positioning for best view**

Under "Edit", select the "Manipulators Tool", and adjust the orientation of the 3D model parallel to the background grid, and zoom to include as many details as possible.

Step 4:   **Curvature color-mapping**

Under "Filters", select "Normals, Curvatures, and Orientation", then "Calculate curvature principle directions" to apply the classic curvature operator.

Under "Filters" menu, select "Normals, Curvatures, and Orientation", then "Discrete Curvatures" to apply the discrete curvature operator.

Step 5:   **Export snapshot**

Select the camera icon ("Save snapshot") and save the image (.png) in "Solid white" background.

Step 6:   **RBG separation**

Import the image into Fiji. Under "Image", select "Color" then "Split Channels" to obtain three Tag Image Files (TIF) of separated RGB channels. The red channel images were inverted using the "Invert LUT" function to show the ridges in black and furrows in white

Figure 17. Combined steps for transforming a 3D scanned fingerprint into a 2D rolled equivalent.

2.4 Image Calibration and Enhancement

A free trial version of CSIpix® Matcher Version 4.0.6 (iSYS Corporation, St. John's, NL, Canada) was obtained and applied for the digital image processing and analysis of fingerprint images. CSIpix® Matcher is a powerful toolkit aimed to assist examiners throughout the entire workflow of friction ridge comparison, containing tools from digital image enhancement to automated minutia detection. All 63 digital photographs and 46 flattened 3D fingerprints (23 red channel images and 23 blue channel images) were processed following the same steps to be calibrated and digitally enhanced if required [Figure 18]. In this experiment, the digital image enhancement was only performed using a local histogram equalization function in the CSIpix® Matcher for consistency. The function equally re-distributes the gray level values within a defined area[44], yielding a high-contrast result image [Figure 19]. The flattened 3D fingerprint images from RGB separation were already in black and white [Figure 16], and no further enhancement was attempted.

Step 1:	**Calibration**

Load the target image as "Left Image". Under "Calibrate", select "Black Ticks (mm)" to automatically search for ruler scale within the photograph. For flattened 3D fingerprints, "Manual Calibration" was used, and a 10 mm segment was manually selected on the background grid.

Step 2:	**Resample**

Under "Resample", select "500 DPI" to allow automatic minutiae detection.

Step 3:	**Digital enhancement (photographs only)**

Under "Enhance", select "Local Equalization" with "Radius" of 5 pixels, then select "Color to Greyscale" and "Luminance" to convert into greyscale scale image.

Step 4:	**Rotating and cropping**

"Rotate" and "Crop" tools were used to orient and maximize the fingerprint portion.

Step 5:	**Export file**

Save "Left Image" as Wavelet Scalar Quantization (WSQ) Bitmap Image

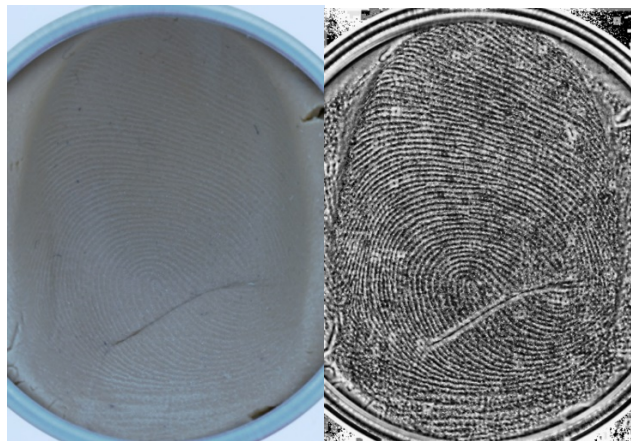**Figure 18. Steps for image calibration and enhancement in CSIpix® Matcher.**

Figure 19. Example of digital enhancement by local equalization. Photograph of an impression in plumber's putty was calibrated, resized, and cropped to the optimal view (left). Local histogram equalization of 5 pixels radius and grayscale transformation were applied to obtain a final black and white image (right).

29

2.5 Automated Minutia Detection and Quality Scores

2.5.1 CSIpix® Matcher

Minutiae counts and match scores were collected using CSIpix® Matcher. The match score was the resulting value from the matching algorithm. The score was calculated based on the number of corresponding minutiae between the left and right images and the relative locations of minutiae, which essentially represents the number of minutiae that makes up the matched pattern[44] [Figure 20]. A reference image of the left or right thumbprint [Figure 5] was loaded as "Right Image", and the calibrated target image was loaded on the left. Minutiae in the left and right images were detected with an "Auto Threshold" of 50 to ensure results with higher quality than the default setting of 20. "Match (Left to Right)" was performed with restricted search angle -15 to 15 degrees to reduce faulty matches as both images were already set at the same orientation. Minutiae count and the highest score of matched regions, or the match score, were recorded for each image. The validity of each match result was manually examined. A *faulty match* was assigned when noncorresponding minutiae from left and right images were mistakenly matched by the algorithm, i.e., matched minutiae were from different regions of the same fingerprint. In the case of a faulty match, the match score was recorded as zero as no true corresponding minutia was found.
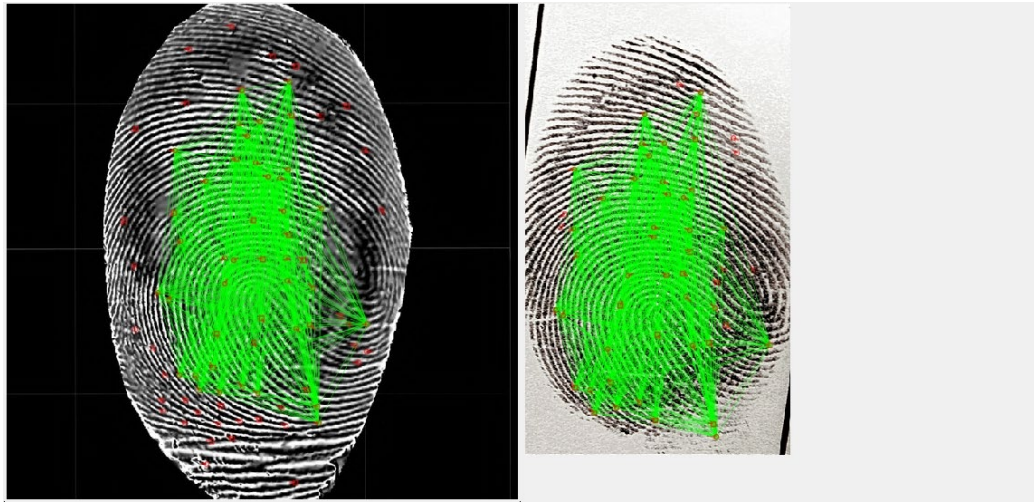
Figure 20. Comparison view of a flattened 3D fingerprint scan (left) to an inked reference impression (right) in CSIpix® Matcher. The depicted pair of images achieved a match score of 38.021, while 82 minutiae (marked in red dots) were detected for the left image and 52 for the right.

2.5.2 NFIQ 2.0

NIST Fingerprint Image Quality Version 2.0 (NFIQ2) (Elham Tabassi, National Institute of Standards and Technology) was employed to assess the actionable quality of fingerprint images, a score of which can be used as the basis for determining whether it is worthwhile to employ an examiner to conduct further analysis. The software takes the input of a BMP or WSQ image of a plain fingerprint captured at 500 dot-per-inch (dpi) and generates a numerical quality score (0-100) based on features including minutiae count, minutiae quality, ridge valley uniformity, and local clarity score[45]. The original source code of NFIQ2 was built on a virtual machine running CentOS 6, a Linux distribution, following the steps described on the development website[45]. In total, 109 WSQ images (63 photographs and 46 flattened 3D fingerprints) were processed by NFIQ2 to obtain a numerical quality score for each image.

2.6 3D Shape Comparison

An STL file can be visualized as a cloud of data points in 3D space. Once two 3D models are set at the same orientation in 3D space, statistical analysis can be performed on the point clouds to determine the average distance and highlight regions with different geometry (e.g., dents or cracks on a surface). Four levels of shape comparison based on a theoretically increasing disparity were performed: same 3D scan (Level I), two 3D scans of the same impression (Level II), two impressions of the same fingerprint in the same material (Level III), two impressions of different fingerprints in the same material (Level IV). Level I and II were designed to assess the robustness of the comparison algorithm and the 3D scanning process. Level III and IV aimed to explore the potential of point cloud comparison for fingerprint individualization and set a threshold for non-matches. The point cloud comparisons were performed using CloudCompare following a customized procedure, which entailed two main steps: 3D clouds registration and calculation. The registration step aligns an 3D fingerprint (aligned) to another 3D fingerprint (reference) in space to achieve maximum overlap [Figure 21], and the calculation step measures the distance between each pair of registered points and calculates the average distance. While using the "Fine Registration" function, the "RMS difference" was set to 1.0e-20 for high accuracy, and "Random sampling limit" was set to 1,000,000 to include all data points. In "General parameters", "Octree level" was set to 8 instead of "Auto" for consistency. Every comparison pair was reciprocally calculated, i.e. the roles of *aligned* and *reference* were switched.

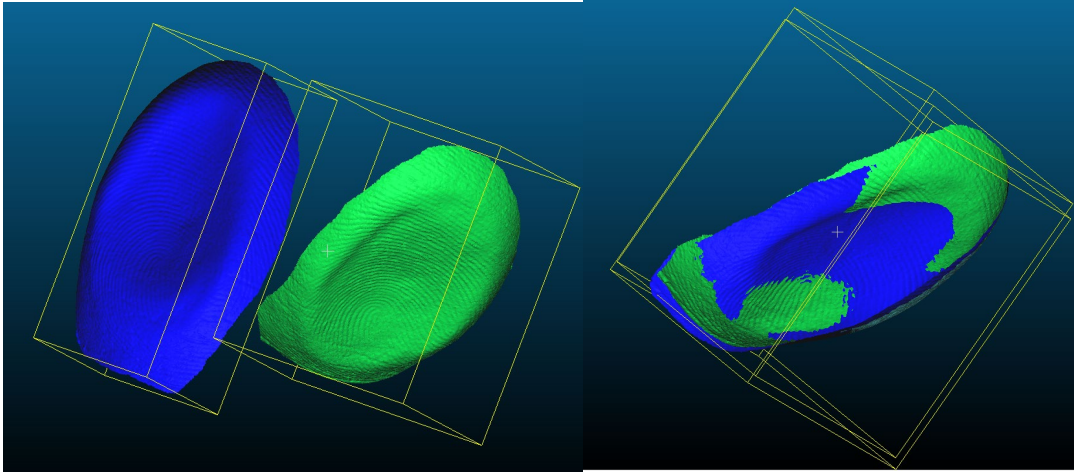**Figure 21. 3D clouds registration of two 3D scanned fingerprints.** The registration algorithm re-orients the *aligned* object (blue) to maximize the spatial overlap with the *reference* object (blue). The mean cloud distance between the two objects was calculated at the finished orientation (right). In theory, 3D impressions of similar shape would yield high overlaps and low mean cloud distance.

3. RESULTS

Twenty different pliable materials were tested as an attempt to account for the diverse physical properties of substrate materials. Fingerprint impressions of reasonable quality could not be created in Materials 11-18 [Table 1] due to one or more of the following reasons: (1) material was adhesive to skin, (2) material deformed at room temperature, (3) short window for fingerprint deposition, and (4) material was hazardous to handle. The different putties and casting materials were among the best for preserving fingerprint impressions for the purposes of this study. The sealing wax, as suggested by Francis Galton[6], was easy and safe to the finger. The same applies to the red dental modeling compound, which was designed to melt at a temperature safe to human skin. However, candle waxes and the gray dental modeling compound could cause burn injuries if not handled properly. For repeatable experiments, the more ephemeral substrates (e.g. grease, ointment) were not considered due to storage difficulties during hot, humid summer weather in Boston.

A total of 25 plastic fingerprint impressions were created, 21 of which were photographed in triplicate, and all 25 impressions were 3D scanned to obtain 33 STL files in total [Table 2]. Scans 32 and 33 were captured with a handheld Artec Space Spider 3D scanner to compare with the 3D scans from the inEos X5® desktop unit. Repeated scans were performed on several impressions with high visual quality, but were only used for point cloud comparisons. Minutiae counts, match scores, and NFIQ2 scores are pooled by

the method utilized. For brevity, the following acronyms were given to address each method:

3CB - Blue channel image of extracted 3D features using the Classic operator
3CR - Red channel image of extracted 3D features using the Classic operator
3DB - Blue channel image of extracted 3D features using the Discrete operator
3DR - Red channel image of extracted 3D features using the Discrete operator
2UP - Unenhanced 2D Photograph
2EP - Enhanced 2D Photograph

3.1 Minutiae Counts

All fingerprint images obtained with 3D scanning methods had positive minutiae counts ranging from 20 (Scan 2, chewed gum, 3CB and 3CR) to 114 (Scan 15, pomade, 3DR) [Figure 22]. Before digital image enhancement, 9 out of 21 2D photographs yielded minutiae counts equal to or below 10, and no minutia was detected for 4 of the 9 photographs in CSIpix® Matcher. After enhancement, all photographs had positive minutiae counts ranging from 10 (Photoset 2, chewed gum, 2EP) to 116 (Photoset 6, modeling clay, 2EP). Only the highest minutiae count of each photoset was chosen for the comparison.

The paired difference statistical analysis was performed using a Wilcoxon signed-rank test[46]. The test is essentially a non-parametric alternative to the paired Student's t-test, i.e., no assumption of normal distribution. Digital enhancement significantly increased the minutiae counts of the photographs ($z = -3.4931$, $p < 0.0005$). Among the flattened 3D fingerprints, the red channel images (3CR and 3DR) contained significantly higher minutiae counts than the blue channel images (3DB and 3CB) ($z = -4.4436$, $p < 0.00001$), and there was no significant difference between the minutiae counts using classic curvature

35

operator and discrete curvature operator ($p > 0.05$). No significant difference was observed between the minutiae counts of flattened 3D fingerprints (3CR and 3DR) and enhanced 2D photographs (2EP) ($p > 0.05$).
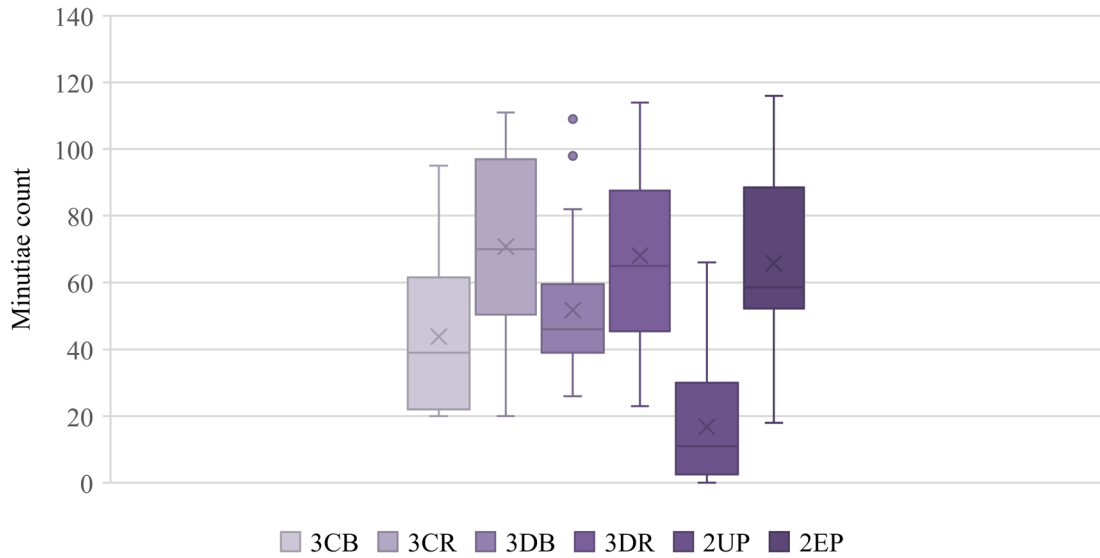
Figure 22. Minutiae counts for the fingerprint images acquired with various methods. Digital enhancement (2EP) enabled the visualization of additional minutiae from the unenhanced photographs (2UP). Red channel images (3CR and 3DR) yielded a significantly higher minutiae count than their corresponding blue channel images (3CB and 3DB). 3D scanning and 2D photography captured a comparable number of minutiae from these 21 plastic fingerprint impressions. The mean value of each set of data is marked by the cross ("X").

3.2 CSIpix® Match Scores

In this experiment, the match score from CSIpix® Matcher fell within a range of 0 to 44, with 44 being the highest quality in the dataset. No matching can be performed for images with fewer than four detected minutiae. All flattened 3D fingerprints were confirmed to be correctly matched to the reference impressions, except for one image (Scan 16, plumber's putty, 3CB) that was determined to be a faulty match. For the 2EP, 8 out of 63 images yielded faulty matches. Despite having over 90 detected minutiae, Photoset 3

(chewed gum) all yielded faulty matches. Only the highest match score of each photoset was considered for comparison. Wilcoxon signed-rank test was performed to determine the significance of the differences in quality score between the methods [Figure 23]. Red channel images (3CR and 3DR) achieved significantly higher match scores than the corresponding blue channel images (3CB and 3DB) ($z = -4.6447$, $p < 0.00001$). Discrete curvature operator (3DB and 3DR) produced significantly higher match scores than the classic curvature operator (3CB and 3CR) ($z = -3.9445$, $p < 0.0001$). When comparing the best of 3D methods to 2EP, 3DR yielded significantly higher match scores ($z = -2.2071$, $p = 0.0271$).

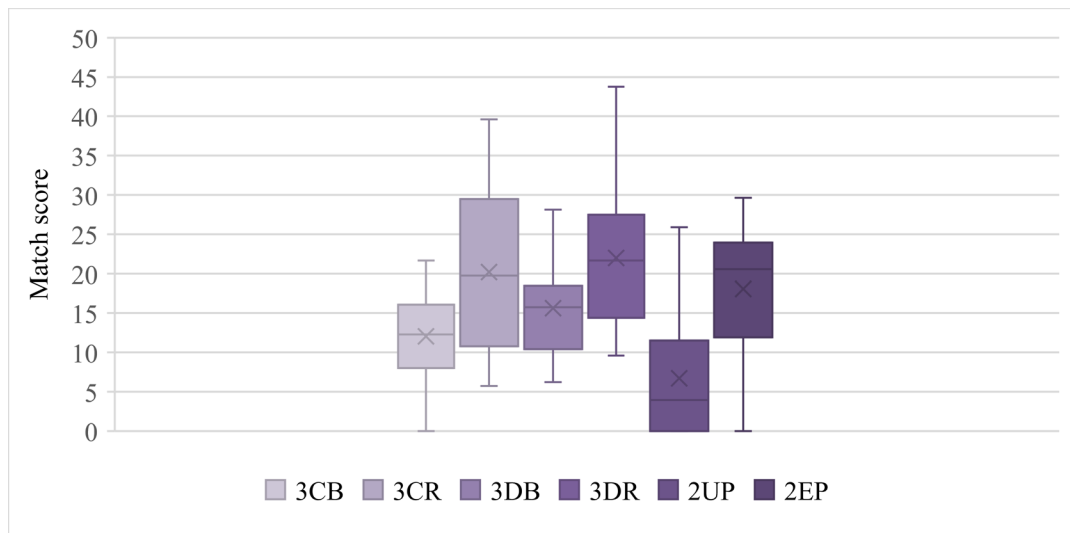**Figure 23. CSIpix® match scores for fingerprint images acquired with various methods.** The red channel image of extracted 3D features using discrete curvature (3DR) achieved the highest match scores. Red channel images of flattened 3D fingerprints (3CR and 3DR) achieved higher match scores than their corresponding blue channel images (3CB and 3DB). The mean value of each set of data is marked by the cross ("X").

3.3 NFIQ 2.0 Quality Scores

The final score of NFIQ2 comes from the integration of several quality scores, which could be acquired along with the individual image quality scores from the log of each command execution. The overall distribution of the NFIQ2 scores is shown in Figure 24. The highest NFIQ2 score achieved among all images was 65 out of 100 (Photoset 14, red dental modeling compound, 2EP). The red channel images (3DR and 3CR) achieved significantly higher NFIQ2 scores than their corresponding blue channel images (3DB and 3CB), and the classic curvature operator (3CB and 3CR) produced significantly higher NFIQ2 scores than the discrete curvature operator (3DB and 3DR) ($z = -2.657$, $p < 0.01$). In contrast to the trend observed in minutiae counts and match scores, 2EP scored the highest among all methods with NFIQ2 ($z = -2.937$, $p < 0.005$, compared with 3CR).
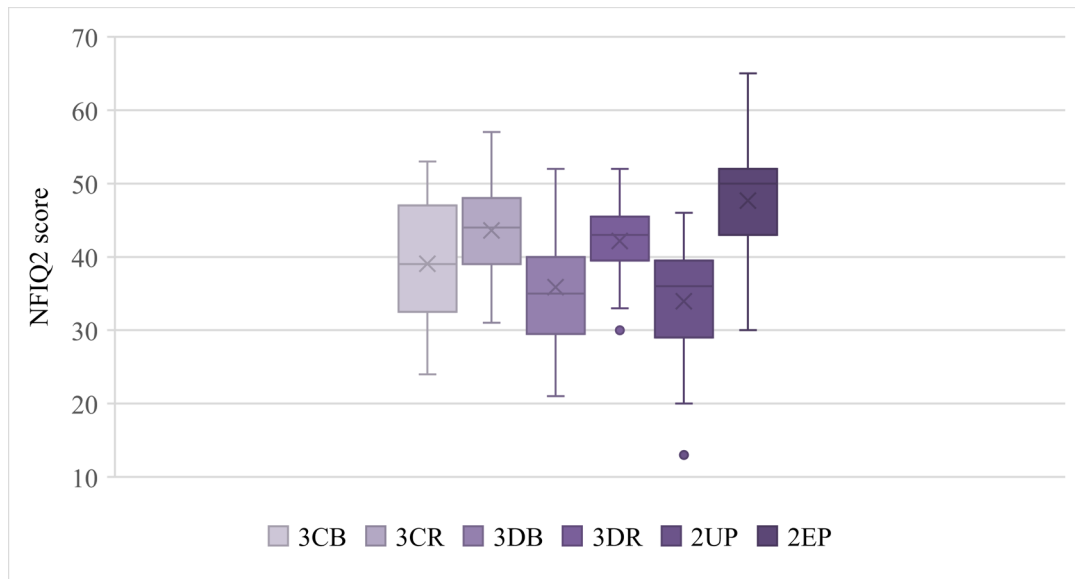

Figure 24. NFIQ 2.0 scores for fingerprint images acquired with various methods. Enhanced 2D photographs (2EP) achieved the highest NFIQ2 scores among all methods, while red channel images with classic curvature operator (3CR) ranked highest among the 3D methods. The mean value of each set of data is marked by the cross ("X").

3.4 3D Shape Comparison

In total, 31 Level I comparisons, six pairs of Level II comparisons, 27 pairs of Level III comparisons, and 11 pairs of Level IV comparisons were conducted, exhausting all possible combinations among Scan 1 to 31 [Table 2]. CloudCompare was efficient at aligning two identical scans to a 100% spatial overlap, indicated by the zero values of standard deviation in point cloud distance analysis. Repeated scans of one impression (Level II) started to exhibit noise in the point cloud, but at a minimal magnitude that could still be differentiated from Level III and IV [Figure 25]. With standard deviations all below 0.2, the Level II shape comparison results demonstrated the high precision of the 3D scanning procedure. Level III and IV comparisons did not exhibit a significant contrast.
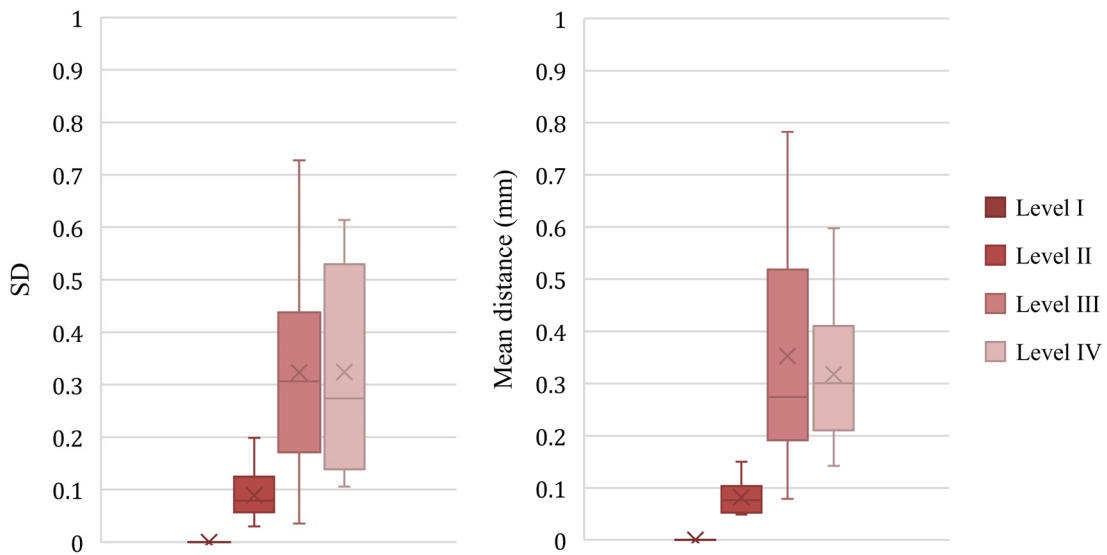
Figure 25. Calculated mean point cloud distances (right) and standard deviations (SD, left) of four levels of shape comparisons with theoretically increasing disparity. Repeated scans of the same impressions yielded significantly lower average distance and standard deviation, allowing a certain degree of individualization of 3D impressions. The mean value of each set of data is marked by the cross ("X").

3.5 Performance of the Artec Space Spider

Two scans of a right thumb impression in white Mikrosil^{TM} (Scan 32 and 33) were captured with the portable Artec Space Spider unit and compared with the scans captured with the benchtop unit (Scan 26 and 27). The portable Artec unit outperformed the inEos X5® in all comparison parameters (minutiae count, match score, and NFIQ2 score), and obtained comparable minutiae counts but higher match scores than the enhanced photographs [Figure 26].

Figure 26. Performance comparisons of two 3D scanners in capturing friction ridge features from one plastic fingerprint impression. A right thumb impression in white Mikrosil™ was 3D scanned with two different 3D scanners. The scans from the Space Spider unit appeared to produce higher minutiae count (top), match score (middle), and NFIQ2 score (bottom) than the inEos X5® unit.

4. DISCUSSION

4.1 Quality of 3D Scanned Fingerprints

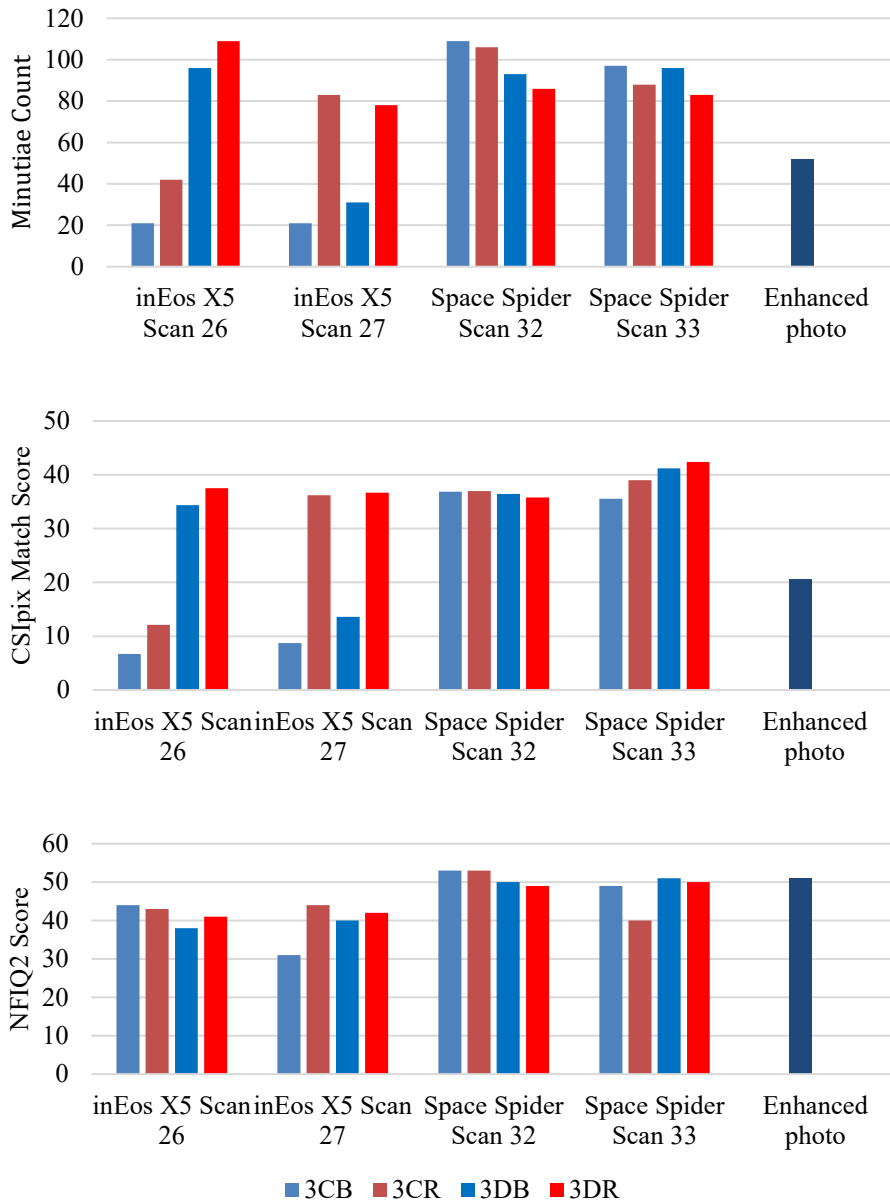The primary objective of this study was to investigate whether 3D scanning could be successfully applied to the documentation of plastic fingerprint impressions and compare 3D scanning to regular photography. The comparison was achieved by the development of a procedure to extract friction ridge features from 3D scanned fingerprints. The fingerprint image quality of red and blue color channels processed by two differential geometry operators was evaluated and compared with regular (2D) photography. Overall, 3D scanning and 2D photography obtained comparable minutiae counts from the same fingerprints, but 3D scanning outperformed 2D photography by achieving fewer faulty matches and higher match scores with CSIpix® Matcher. The portable 3D scanner (Artec Space Spider) outperformed the benchtop unit (inEos X5®) in all three comparison parameters.

The actionable quality of each fingerprint image was assessed with NFIQ 2.0, the scores of which indicated that the enhanced 2D photographs (2EP) had the highest actionable quality. When reviewing the NFIQ2 result output, it was discovered that the modified FingerJet FX OSE fingerprint feature extractor (DigitalPersona, Inc.) module of NFIQ2 could not reliably detect minutiae in flattened 3D fingerprints. While the module functioned flawlessly with enhanced photographs, which all received minutiae count of above 100, only 3 out of 88 flattened 3D fingerprints and 8 out of 63 unenhanced 2D photographs received non-zero minutiae counts. Therefore, the NFIQ2 scores do not hold much value for the comparisons between 2D photography and 3D scanning due to the

minutiae detection issue. The observed discrepancy in the minutiae detection in 3D scanned fingerprints might have originated from the NFIQ2 design, as the software was never intended for fingerprint images obtained from sources other than optical sensors[45].

Methods that require a person in order to be carried out are often subject to human error and bias, affecting the reliability of the results. 3D point cloud comparisons were performed to evaluate the reproducibility and repeatability of the 3D documentation method. Repeated 3D scans of the same impressions were found to bear minimal deviation in shape, demonstrating the robustness of operation. However, the point cloud comparison algorithm was found to be highly sensitive to the overall shape of the impression but not significantly affected by the individual friction ridge details embedded within the surface. Furthermore, the 3D clouds registration algorithm could not reliably align the friction ridges on impressions that were in relatively flat surfaces, rendering the point cloud statistics pointless. Due to the above reasons, 3D cloud statistics might not be effective for comparing the friction ridge patterns on two different fingerprints, as the differences in the overall shapes could mask the differences in the friction ridges entirely. However, 3D shape comparison can be useful in the comparison of other types of impressions where the difference in overall shape is more prominent, such as footwear impressions and fractured edges.

4.2 Forensic Implications

3D scanning demonstrated robustness as well as efficiency in the collection of plastic fingerprint impressions. Many limitations of traditional photography could be easily

circumvented by the fundamental features of structured-light 3D scanning. 3D scanners such as the ones in this experiment utilize blue LED as the light source, which allows operations independent of scene lighting, as blue lights are not commonly found among artificial light sources. The mechanism of SLS also eliminates the need for physical scales, as the scanning process records all dimensional information to create an accurate 3D model. The exact point-to-point distances in 3D space can be measured and re-examined any time from the generated 3D model. 3D scanning also compensates the limited depth perception in a single shot by rapidly capturing multiple frames at different focus settings and merging them with sophisticated algorithms.

Introducing 3D scanning into the forensic community could spark many new applications, but also challenges. The primary concern before conducting this study was whether the 3D scanners could capture a fingerprint impression at a resolution high enough to allow visualization of ridge details. The results of the experiments gave an affirmative answer on the Level 2 features, but the visualization of Level 3 features remained elusive. Pore-like development was visualized in the corresponding 3DR-processed image [Figure 27], but could not be confirmed due to the limited resolution. Despite an extensive amount of effort to create fingerprint impressions of high fidelity, the majority of the materials did not preserve small details such as pores [Figure 28]. In this experiment, only the Mikrosil[TM], which has long been applied to the collection of postmortem fingerprints[47], was able to preserve the pores in friction skin. In real cases, accidentally deposited impressions with usable Level 3 details are rare. Therefore, the visualization of pores might not even be an imperative feature for the analysis of plastic fingerprint impressions.

The ability to scan a finger or fingerprint in 3D opens new possibilities to the current fingerprint identification systems. Despite the seemingly unrelated technologies, there is no real compatibility gap between 3D scanning and 2D photography of fingerprints, as was demonstrated in this study. 3D scanned fingerprints can be easily transformed to 2D rolled equivalent images with several other unwrapping models[18,20,48] and imported into the AFIS database. The 3D data enables a new level of fingerprint comparison based on curvature features[49]. If scan resolution allows, the 3D shape and depth of ridges can also become potential targets for analysis.

In the courtroom, 3D visualization technology enables the display of challenging evidence such as gruesome wounds by stripping out the prejudicial graphic depiction of injuries and exhibiting only the relevant geometry to ensure the fairness of the trial proceedings[34,50]. The exact events can also be better reproduced and delivered by placing the subject within a virtual 3D scene using 3D reconstruction[51]. The technology can be applied to a further extent to produce a 3D printed model of the evidentiary item, which helps to keep the jury's attention during lengthy trials and possibly aids their understanding of scientific facts[52]. On the other hand, the same technology can also be re-engineered to deceive fingerprint readers to possibly gain illegal access[53]. As demonstrated in another study, a fabricated 3D fingerprint target was able to produce impressions of high fidelity using a contact-based slap reader[54]. Combining with the improvements in 3D scanning speed and accuracy, duplication of 3D fingerprints is already a reality.
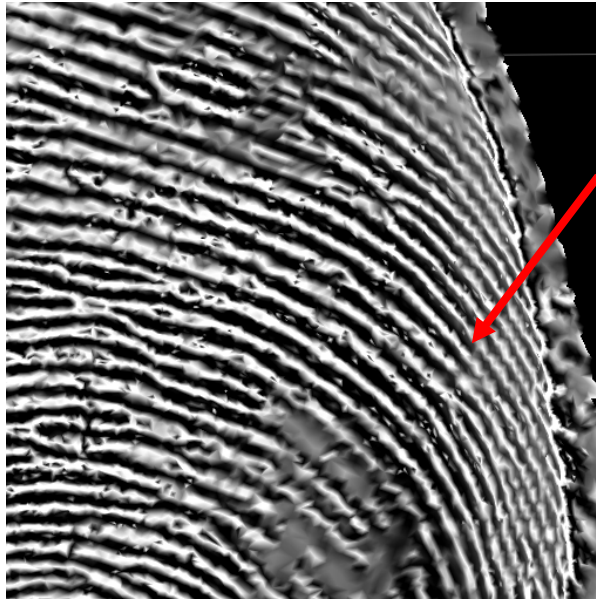
Figure 27. Processed image of a 3D scanned plastic fingerprint impression in white Mikrosil™. Red arrow indicates area with potential development of pores. Image was processed with the 3DR method.
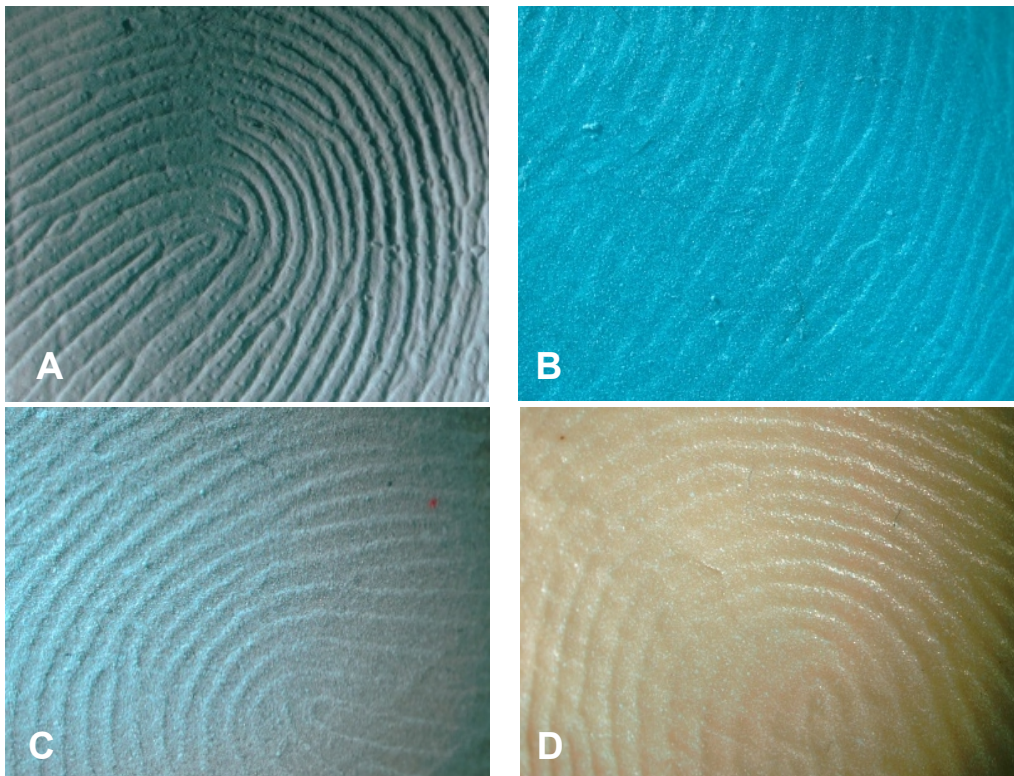
Figure 28. Photomicrographs of 3D fingerprint impressions in four different materials. The photographs were taken with a stereomicroscope at 10X magnification with oblique lighting. Pores were visualized in white Mikrosil™ (A), but not in chewed gum (B), modeling putty (C), or plumber's putty (D).

5. CONCLUSIONS

Traditional 2D photography can be unwieldy and inadequate for the documentation of 3D impression evidence. In this study, prepared plastic fingerprint impressions were successfully captured with structured-light 3D scanners and processed with four methods to allow better visualization of friction ridge features than traditional photography while recording the exact 3D geometry. Traditional photography without digital enhancement was inadequate in capturing friction ridge details in impressions that contain three-dimensional (3D) details. After digital enhancement, 12.7% of the enhanced 2D photographs were incorrectly matched with the reference impressions with CSIpix® Matcher, while the 3DR method achieved the highest match quality among all methods, with minutiae counts all above 23, and yielded no faulty matches. The portable 3D scanner unit (Artec Space Spider) outperformed the benchtop unit (inEos X5®) in minutiae count, match score, and NFIQ2 score within an, albeit small, sample pool. With proper education and training, 3D scanning technology can significantly enhance the ability of forensic scientists to capture, analyze, and search 3D fingerprint impression evidence.

6. DIRECTIONS FOR FUTURE STUDY

As a method targeted for the delicate and immobile impressions at crime scenes, portability is an essential attribute. The potential of the hand-held 3D scanner unit was not fully explored due to limited resources. Although the results of the hand-held unit demonstrated equivalent performance compared to the benchtop unit, it would be more relevant to test realistic crime scene scenarios (e.g., 3D impressions on a vertical wall, curved or irregular surfaces). Future studies could investigate the performance of handheld 3D scanners within the context of a mock crime scene, which should expose more challenges with the collection of plastic prints.

Despite the promising advantages of 3D scanning technology in the documentation of plastic prints, validation studies in a forensic science context are scarce. In contrast to the 3D documentation of injuries and crime scenes where a macroscopic recording of shapes and dimensions would be sufficient for the purpose of documentation and court demonstration, fingerprint analysis relies on minutiae that are beyond the resolving power of many commercial 3D scanners. The mathematical foundations of many 3D mesh processing techniques (e.g., curvature color-mapping and unwrapping algorithm) have long existed but can still appear esoteric to many in the forensic field. Compounded by the general lack of understanding of 3D reconstruction, any manipulation on the raw 3D scan data can and will raise concerns on the validity of the end result. To cope with these concerns, more studies are required to evaluate the validity of the 3D scanning and mesh processing methods in the context of forensic pattern evidence.

Fingerprint analysis is only one of many subdisciplines involving pattern evidence, as pertinent 3D details are common among toolmarks, footwear impressions, tire tracks, and fractured edges. Therefore, it would be natural to extend the potential of 3D scanning technology in the documentation and collection of evidence containing rich 3D features. If successful, 3D scanners could significantly reduce time spent on the camera set-up and revolutionize the comparison process by allowing examiners to freely manipulate the captured 3D models within a virtual 3D space. For impression evidence with a relatively rigid shape, 3D shape comparison, as demonstrated in this study, could be utilized as a comparison method that reports a statistical significance.

LIST OF JOURNAL ABBREVIATIONS

Adv Opt Photonics	Advances in Optics and Photonics
Am Crim Law Rev	American Criminal Law Review
Am J Anat	American Journal of Anatomy
Appl Opt	Applied Optics
Comput Graph Forum	Computer Graphics Forum
Forensic Sci Int	Forensic Science International
IEEE Trans Inf Forensics Secur	IEEE Transactions on Information Forensics and Security
IEEE Trans Pattern Anal Mach Intell	IEEE Transactions on Pattern Analysis and Machine Intelligence
Image Vis Comput	Image and Vision Computing
ISPRS Arch Photogramm Remote Sens Spat Inf Sci	ISPRS Archives of Photogrammetry, Remote Sensing and Spatial Information Sciences
ISPRS J Photogramm Remote Sens	ISPRS Journal of Photogrammetry and Remote Sensing
J Crim Law Criminol	Journal of Criminal Law and Criminology
J Forensic Identif	Journal of Forensic Identification
J Forensic Leg Med	Journal of Forensic and Legal Medicine
J Forensic Radiol Imaging	Journal of Forensic Radiology and Imaging
J Forensic Sci	Journal of forensic sciences
Law Hum Behav	Law and Human Behavior

Nat Methods	Nature Methods
Pattern Recognit	Pattern Recognition
Z Morphol Anthropol	Zeitschrift für Morphologie und Anthropologie

BIBLIOGRAPHY

1. Minakata K. The antiquity of the "finger-print" method. Nature. 1894;51(1313):199–200.

2. Giles HA. Phrenology, Physiognomy, and Palmistry. In: Adversaria Sinica. Shanghai: Kelly & Walsh Ltd., 1905; 183.

3. Holder EH, Robinson LO, Laub JH. The Fingerprint Sourcebook. Washington, DC: U.S. Dept. of Justice, Office of Justice Programs, National Institute of Justice, 2012.

4. Ashbaugh DR. Quantitative-qualitative friction ridge analysis : an introduction to basic and advanced ridgeology. 1st Editio. Boca Raton, FL: CRC Press, 1999.

5. Herschel W. The Origin of Finger-Printing. London, H. Milford: Oxford University Press, 1916.

6. Galton F. Finger prints. London: Macmillan and Co., 1892.

7. Polson CJ. Finger Prints and Finger Printing. An Historical Study. J Crim Law Criminol 1950;41(4):495.

8. People v. Jennings, 96 N.E. 1077, 252 Ill. 534 (1911).

9. Cole SA. Grandfathering Evidence: Fingerprint Admissibility Rulings from Jennings to Llera Plaza and Back Again. Am Crim Law Rev 2004;41(3):1189–276.

10. Daubert v. Merrell Dow Pharmaceuticals, 509 U.S. 579 (1993).

11. Community Committee on Identifying the Needs of the Forensic Sciences, National. Strenghening Forensic Science in the United States: A Path Forward. Washington, DC: 2009.

12. Whipple IL, Wilder HH. The Ventral Surface of the Mammalian Chiridium with special reference to the conditions found in man. Z Morphol Anthropol 1904;7(2):261–368.

13. Wertheim K, Maceo A. The critical stage of friction ridge and pattern formation. J Forensic Identif 2002;52(1):35–85.

14. Hale AR. Morphogenesis of volar skin in the human fetus. Am J Anat 1952;91(1):147–81.

15. Lin CH, Liu JH, Osterburg JW, Nicol JD. Fingerprint comparison. I: Similarity of fingerprints. J Forensic Sci 1982;27(2):290–304.

16. Hawthorne MR. Fingerprints: Analysis and Understanding. Boca Raton, FL: CRC Press, 2009.

17. Stimac JT. Plastic fingerprint impressions : An inked approach. J Forensic Identif 1998;48(5):574.

18. Fatehpuria A, Lau DL, Hassebrook LG. Acquiring a 2D rolled equivalent fingerprint image from a non-contact 3D finger scan. In: Defense and Security Symposium. Orlando, FL: 2006; 62020C.

19. Kumar A, Kwong C. Towards contactless, low-cost and accurate 3D fingerprint identification. IEEE Trans Pattern Anal Mach Intell 2015;37(3):681–96.

20. Wang Y, Hassebrook LG, Lau DL. Data acquisition and processing of 3-D fingerprints. IEEE Trans Inf Forensics Secur 2010;5(4):750–60.

21. Lin C, Kumar A. Contactless and partial 3D fingerprint recognition using multi-view deep representation. Pattern Recognit 2018;83:314–27.

22. Galton F. Personal Identification and Description. Nature 1888;38(973):173–7.

23. Jain AK, Chen Y, Demirkus M. Pores and ridges: High-resolution fingerprint matching using level 3 features. IEEE Trans Pattern Anal Mach Intell 2007;29(1):15–27.

24. SWGFAST. Document #8 Standard for the Documentation of Analysis, Comparison, Evaluation, and Verification (ACE-V) (Latent) [Internet]. 2012 [cited 2018 Sep 18];1–14. Available from: http://clpex.com/swgfast/documents/documentation/121124_Standard-Documentation-ACE-V_2.0.pdf

25. SWGFAST. Document #10 Standards for Examining Friction Ridge Impressions and Resulting Conclusions (Latent/Tenprint) [Internet]. 2011 [cited 2018 Sep 18];16. Available from: http://clpex.com/swgfast/documents/examinations-conclusions/130427_Examinations-Conclusions_2.0.pdf

26. Ulery BT, Hicklin RA, Roberts MA, Buscaglia J. Measuring What Latent Fingerprint Examiners Consider Sufficient Information for Individualization Determinations. PLoS One 2014;9(11):e110179.

27. Brown CM. Computer vision and natural constraints. Science (80-) 1984;224(4655):1299–305.

28. Agarwal S, Snavely N, Simon I, Seitz SM, Szeliski R. Building Rome in a day. In: 2009 IEEE 12th International Conference on Computer Vision. Kyoto, Japan: IEEE, 2009; 72–9.

29. Komar DA, Davy-Jow S, Decker SJ. The Use of a 3-D Laser Scanner to Document Ephemeral Evidence at Crime Scenes and Postmortem Examinations. J Forensic Sci 2012;57(1):188–91.

30. Thali MJ, Yen K, Schweitzer W, Vock P, Boesch C, Ozdoba C, et al. Virtopsy, a new imaging horizon in forensic pathology: virtual autopsy by postmortem multislice computed tomography (MSCT) and magnetic resonance imaging (MRI)--a feasibility study. J Forensic Sci 2003;48(2):386–403.

31. Georgopoulos A, Ioannidis C, Valanis A. Assessing the Performance of a Structured Light Scanner. ISPRS Arch Photogramm Remote Sens Spat Inf Sci 2010;XXXVIII(5):250–5.

32. Geng J. Structured-light 3D surface imaging: a tutorial. Adv Opt Photonics 2011;3(2):128–60.

33. Shamata A, Thompson T. Documentation and analysis of traumatic injuries in clinical forensic medicine involving structured light three-dimensional surface scanning versus photography. J Forensic Leg Med 2018;58:93–100.

34. Errickson D, Thompson TJU, Rankin BWJ. The application of 3D visualization of osteological trauma for the courtroom: A critical review. J Forensic Radiol Imaging 2014;2(3):132–7.

35. Wang Y, Hassebrook L, Lau D. Noncontact, depth-detailed 3D fingerprinting. SPIE Newsroom 2009;3–5.

36. Mulawka M. Evaluation of The Use of A Contactless, Three-Dimensional Scanner for Collecting Postmortem Fingerprints from Unidentified Human Remains [Internet]. 2016 [cited 2019 Mar 21];National Institute of Justice Grant Award # 2016-D. Available from: https://external.ojp.usdoj.gov/selector/awardDetail?awardNumber=2016-DN-BX-0180&fiscalYear=2016&applicationNumber=2016-90345-TX-IJ&programOffice=NIJ&po=NIJ

37. Rocchini C, Cignoni P, Montani C, Pingi P, Scopigno R. A low cost 3D scanner based on structured light. Comput Graph Forum 2001;20(3):299–308.

38. Salvi J, Pagès J, Batlle J. Pattern codification strategies in structured light systems. Pattern Recognit 2004;37(4):827–49.

39. Graham CA, Akoglu KG, Lassen AW, Simon S. Epic dimensions: A comparative analysis of 3d acquisition methods. ISPRS - Int Arch Photogramm Remote Sens Spat Inf Sci 2017;XLII-2/W5(2W5):287–93.

40. Koenderink JJ, van Doorn AJ. Surface shape and curvature scales. Image Vis Comput 1992;10(8):557–64.

41. Cignoni P, Callieri M, Corsini M, Dellepiane M, Ganovelli F, Ranzuglia G. MeshLab: an Open-Source Mesh Processing Tool. In: Eurographics Italian Chapter Conference 2008: Salerno, Italy. 2008; 129–36.

42. Meyer M, Desbrun M, Schröder P, Barr AH. Discrete Differential-Geometry Operators for Triangulated 2-Manifolds. In: Hege H-C, Polthier KP, editors. Visualization and Mathematics III. Springer-Verlag Berlin Heidelberg, 2003; 35–57.

43. Schindelin J, Arganda-Carreras I, Frise E, Kaynig V, Longair M, Pietzsch T, et al. Fiji: An open-source platform for biological-image analysis. Nat Methods 2012;9(7):676–82.

44. CSIpix V4 Comparator, Matcher & Case AFIS User Guide. St. John's, NL, Canada: Intelligent System Solutions Corporation, 2018; 54–6.

45. Tabassi E. Development of NFIQ 2.0 [Internet]. 2012 [cited 2018 Sep 18];Available from: https://www.nist.gov/services-resources/software/development-nfiq-20

46. Wilcoxon F. Individual Comparisons by Ranking Methods. Biometrics Bull 1945;1(6):80–3.

47. Bay A.L. J. Additional use for mikrosil(TM) casting material. J Forensic Identif 1998;48:130–2.

48. Wang Y, Lau DL, Hassebrook LG. Fit-sphere unwrapping and performance analysis of 3D fingerprints. Appl Opt 2010;49(4):592.

49. Liu F, Zhang D, Shen L. Study on novel Curvature Features for 3D fingerprint recognition. Neurocomputing 2015;168:599–608.

50. Bright DA, Goodman-Delahunty J. Gruesome Evidence and Emotion: Anger, Blame, and Jury Decision-Making. Law Hum Behav 2006;30(2):183–202.

51. Buck U, Naether S, Braun M, Bolliger S, Friederich H, Jackowski C, et al. Application of 3D documentation and geometric reconstruction methods in traffic accident analysis: With high resolution surface scanning, radiological MSCT/MRI

scanning and real data based animation. Forensic Sci Int 2007;170(1):20–8.

52.   Baier W, Warnett JM, Payne M, Williams MA. Introducing 3D Printed Models as Demonstrative Evidence at Criminal Trials. J Forensic Sci 2018;63(4):1298–302.

53.   Matsumoto T, Matsumoto H, Yamada K, Hoshino S. Impact of artificial "gummy" fingers on fingerprint systems. Proc SPIE 2002;4677:275–89.

54.   Arora SS, Jain AK, Paulter NG. 3D Whole Hand Targets: Evaluating Slap and Contactless Fingerprint Readers. In: 2016 International Conference of the Biometrics Special Interest Group (BIOSIG). IEEE, 2016; 1–8.

CURRICULUM VITAE